J|A|C|S
ARTICLES
Published on Web 11/11/2005

Intermolecular Charge Transfer between Heterocyclic Oligomers. Effects of Heteroatom and Molecular Packing on Hopping Transport in Organic Semiconductors

Geoffrey R. Hutchison,*,† Mark A. Ratner,* and Tobin J. Marks*

Contribution from the Department of Chemistry and the Materials Research Center, Northwestern University, Evanston, Illinois 60208-3113

Received May 24, 2005; E-mail: grh25@cornell.edu; ratner@chem.northwestern.edu; t-marks@northwestern.edu

Abstract: For electron or hole transfer between neighboring conducting polymer strands or oligomers, the intrinsic charge-transfer rate is dictated by the charge-resonance integral and by the reorganization energy due to geometric relaxation. To explain conduction anisotropy and other solid-state effects, a multivariate, systematic analysis of bandwidth as a function of intermolecular orientations is undertaken for a series of oligoheterocycles, using first-principles methods. While cofacial oligomers show the greatest bandwidths at a given intermolecular C−C contact distance, for a fixed center-to-center intermolecular distance, tilted π-stacking increases π-overlap (particularly for LUMO orbitals) and decreases electrostatic repulsion, yielding optimum tilt angles for packing of ~40−60° at small intermolecular separations. The calculations also reveal that bandwidths and intrinsic mobilities of holes and electrons in conjugated oligoheterocycles can be quite comparable.

I. Introduction

Conjugated organic materials are of immense current interest, both for the intrinsic scientific challenges they present and for the technologies they offer, including light-emitting diodes,[1] photovoltaics,[2] field-effect transistors,[3] and other elements of "plastic electronics". Over nanoscopic and mesoscopic length scales, the mechanisms of charge transfer in organic conductive materials are subject to considerable uncertainty and likely differ substantially for different materials.[4,5] However, near room temperature, conjugated oligomers and polymers are known to transport charge via a thermally activated hopping-type mechanism,[5,6] which depends on the relative orientations and solid-state packing of the species involved.[6−10]

The charge-transfer process (for holes or electrons) between spatially separated molecules (i.e., either two oligomers or two polymer chains) can be summarized by either of the following reactions:

$$\begin{aligned} M + M^+ &\rightarrow M^+ + M \\ M + M^- &\rightarrow M^- + M \end{aligned} \tag{1}$$

where M represents the molecule undergoing charge transfer, and the M^+ or M^- species contain either the hole or electron, respectively. If the temperature is sufficiently high to reasonably treat vibrational modes classically, previous work yields the following Marcus-type expression for the hole (or electron) charge-transfer rate:[11,12]

$$k_{\text{transfer}} = \left(\frac{\pi}{\lambda k_B T}\right)^{1/2} \frac{V^2}{\hbar} \exp\left(-\frac{\lambda}{4 k_B T}\right) \tag{2}$$

where T is the temperature, $\hbar$ the Planck constant, and k_B the

† Current address: Department of Chemistry and Chemical Biology, Cornell University, Baker Laboratory, Ithaca, New York 14853-1301.

(1) (a) Ho, P. K. H.; Kim, J.-S.; Burroughes, J. H.; Becker, H.; Li, S. F. Y.; Brown, T. M.; Cacialli, F.; Friend, R. H. *Nature* **2000**, *404*, 481. (b) Pinner, D. J.; Friend, R. H.; Tessler, N. *Appl. Phys. Lett.* **2000**, *76*, 1137. (c) Inganäs, O.; Berggren, M.; Andersson, M. R.; Gustafsson, G.; Hjertberg, T.; Wennerström, O.; Dyreklev, P.; Granström, M. *Synth. Met.* **1995**, *71*, 2121.
(2) (a) Ding, L.; Jonforsen, M.; Roman, L. S.; Andersson, M. R.; Inganäs, O. *Synth. Met.* **2000**, *110*, 113. (b) Granström, M.; Petrisch, K.; Arias, A. C.; Lux, A.; Andersson, M. R.; Friend, R. H. *Nature* **1998**, *395*, 257.
(3) (a) Würthner, F. *Angew. Chem., Int. Ed.* **2001**, *40*, 1037. (b) Garnier, F. *Chem. Phys.* **1998**, *227*, 253. (c) Katz, H. E. *J. Mater. Chem.* **1997**, *7*, 369.
(4) (a) Prigodin, V. N.; Epstein, A. J. *Synth. Met.* **2001**, *125*, 43. (b) Joo, J.; Lee, J. K.; Baeck, J. S.; Kim, K. H.; Oh, E. J.; Epstein, J. *Synth. Met.* **2001**, *117*, 45. (c) Hilt, O.; Reedijk, J. A.; Martens, H. C. F.; Brom, H. B.; Michels, M. A. J. *Phys. Status Solidi B* **2000**, *218*, 279. (d) Reedijk, J. A.; Martens, H. C. F.; Brom, H. B.; Michels, M. A. J. *Phys. Rev. Lett.* **1999**, *83*, 3904. (e) Kohlman, R. S.; Epstein, A. J. In *Handbook of Conducting Polymers*, 2nd ed.; Skotheim, T. A., Elsenbaumer, R. L., Reynolds, J. R., Eds.; Marcel Dekker: New York, 1998; pp 85. (f) Menon, R.; Yoon, C. O.; Moses, D.; Heeger, A. J. In *Handbook of Conducting Polymers*, 2nd ed.; Skotheim, T. A., Elsenbaumer, R. L., Reynolds, J. R., Eds.; Marcel Dekker: New York, 1998; p 27. (g) Epstein, A. J. *Mater. Res. Bull.* **1997**, *22*, 16.
(5) (a) Epstein, A. J.; Lee, W. P.; Prigodin, V. N. *Synth. Met.* **2001**, *117*, 9. (b) Reedijk, J. A.; Martens, H. C. F.; van Bohemen, S. M. C.; Hilt, O.; Brom, H. B.; Michels, M. A. J. *Synth. Met.* **1999**, *101*, 475. (c) Mott, N. F.; Davis, E. A. *Electronic Processes in Non-Crystalline Materials*, 2d ed.; Oxford University Press: Oxford, 1979.
(6) (a) Pope, M.; Swenberg, C. E. *Electronic Processes in Organic Crystals and Polymers*, 2nd ed.; Oxford University Press: New York, 1999. (b) Pope, M.; Swenberg, C. E. *Electronic Processes in Organic Crystals*; Oxford University Press: New York, 1982.
(7) Cheng, Y. C.; Silbey, R. J.; da Silva, D. A.; Calbert, J. P.; Cornil, J.; Brédas, J. L. *J. Chem. Phys.* **2003**, *118*, 3764.
(8) Brédas, J. L.; Calbert, J. P.; da Silva, D. A.; Cornil, J. *Proc. Natl. Acad. Sci. U.S.A.* **2002**, *99*, 5804.
(9) Brédas, J. L.; Beljonne, D.; Cornil, J.; Calbert, J. P.; Shuai, Z.; Silbey, R. *Synth. Met.* **2001**, *125*, 107.
(10) Cornil, J.; Beljonne, D.; Calbert, J. P.; Brédas, J. L. *Adv. Mater.* **2001**, *13*, 1053.
(11) Berlin, Y. A.; Hutchison, G. R.; Rempala, P.; Ratner, M. A.; Michl, J. *J. Phys. Chem. A* **2003**, *107*, 3970.

10.1021/ja0533996 CCC: $30.25

Boltzmann constant. The parameters of key importance in hopping transport are the reorganization energy (λ) accompanying geometric relaxation associated with the charge transfer and the effective electronic coupling matrix element (V) between neighboring species, dictated largely by orbital overlap. The latter is spatially dependent since it describes the overlap of particular orbitals dictated by the mutual separations and orientations of the adjacent molecules. Since the conjugated CC stretching modes are $\sim$1500 cm^{-1}, the classical high-temperature limit assumed in eq 2 is only approximate, and a full quantum mechanical treatment would lower the actual barrier from that computed from λ as described here. Recent work from our group investigated the variation of λ for hole transfer in oligoheterocycles[13] and demonstrated that eq 2 is an entirely reasonable approximation. Similarly, recent work predicting hole mobilities in pentacene via eq 2 yields reasonable agreement with single-crystal experimental measurements.[14]

A key challenge for understanding conductivity in organic π-electronic materials is to identify those structural factors important in charge-transfer rates and their dependence on supramolecular architecture. Particularly noteworthy is the frequently observed anisotropic character of the conductivity,[15] which implies preferred directions for maximum mobility in such materials and suggests that appropriate crystal engineering to enhance π-overlap between molecules may be an attractive route to improving the intrinsic mobility, for example, by suppressing the typical herringbone[16−18] packing of oligothiophenes in favor of parallel eclipsed orientations.

Brédas et al. previously estimated the electronic coupling matrix element V in eq 2 from semiempirical computation of orbital splitting energies in molecular clusters,[8,10] but provided no information on the relative binding energies of particular molecular spatial arrangements. Other work investigated intermolecular interactions with semiempirical methodologies,[19] demonstrated that solid-state hole mobility in arylamines is related to the internal molecular reorganization energy λ,[20] and identified correlations between molecular architecture and internal reorganization energy.[13,21] However, the reorganization energy of a molecular system should not be orientation-dependent and hence cannot explain the anisotropy of conduction.

A number of factors, including heteroatom identity, heterocyclic substituents, bond-length alternation, and conjugation length, have been demonstrated in both experimental and theoretical studies to be important in determining optical properties (particularly optical band gap),[22−24] bandwidth,[24] and the internal reorganization energy of charge transfer[13] in oligoheterocycles. However, there have been no systematic analyses of how structural factors, such as intermolecular geometric orientation, influence bandwidths in such materials, and, in particular, which address how heteroatom identity influences bandwidth or the energetic stability of particular molecular packing arrangements. Such an analysis would provide an assessment of the possible range of charge-transfer rates in such molecular solids, given reported values for the internal reorganization energies. It would also clarify important structural factors required for design of new highly conductive *p*- or *n*-type molecular/polymeric materials. Further, it would provide valuable predictions as to the mobilities expected for different π-stacking motifs, such as cofacial versus herringbone versus tilted π-stacks.

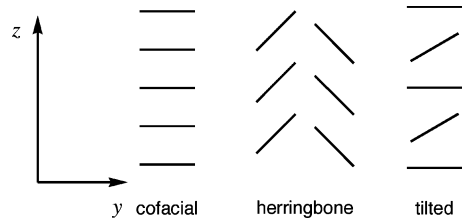

To this end, we present here a multidimensional, systematic comparative study of the effects of structural parameters, such as heteroatom identity, oligomer dimensions, and packing arrangement on orbital splittings for holes (HOMO) and electrons (LUMO) in three series of heterocyclic oligomers

(12) (a) Bixon, M.; Jortner, J. *Adv. Chem. Phys.* **1999**, *106*, 35. (b) Newton, M. D. *Adv. Chem. Phys.* **1999**, *106*, 303. (c) Barbara, P. F.; Meyer, T. J.; Ratner, M. A. *J. Phys. Chem.* **1996**, *100*, 13148. (d) Marcus, R. A.; Eyring, H. *Annu. Rev. Phys. Chem.* **1964**, *15*, 155. (e) McConnell, H. M. *J. Chem. Phys.* **1961**, *35*, 508. (f) Hush, N. S. *J. Chem. Phys.* **1958**, *28*, 962. (g) Marcus, R. A. *J. Chem. Phys.* **1956**, *24*, 966. (h) Marcus, R. A. *Rev. Mod. Phys.* **1993**, *65*, 599. (i) Newton, M. D.; Sutin, N. *Annu. Rev. Phys. Chem.* **1984**, *35*, 437.
(13) Hutchison, G. R.; Ratner, M. A.; Marks, T. J. *J. Am. Chem. Soc.* **2005**, *127*, 2339.
(14) Deng, W. Q.; Goddard, W. A. *J. Phys. Chem. B* **2004**, *108*, 8614.
(15) (a) Silerova, R.; Kalvoda, L.; Neher, D.; Ferencz, A.; Wu, J.; Wegner, G. *Chem. Mater.* **1998**, *10*, 2284. (b) Adams, P. N.; Laughlin, P. J.; Monkman, A. P.; Bernhoeft, N. *Solid State Commun.* **1994**, *91*, 875. (c) Ostrick, J. R.; Dodabalapur, A.; Torsi, L.; Lovinger, A. J.; Kwock, E. W.; Miller, T. M.; Galvin, M.; Berggren, M.; Katz, H. E. *J. Appl. Phys.* **1997**, *81*, 6804.
(16) (a) Facchetti, A.; Deng, Y.; Wang, A.; Koide, Y.; Sirringhaus, H.; Marks, T. J.; Friend, R. H. *Angew. Chem., Int. Ed.* **2000**, *39*, 4547. (b) Facchetti, A.; Mushrush, M.; Katz, H. E.; Marks, T. J. *Adv. Mater.* **2003**, *15*, 33. (c) Jones, B. A.; Ahrens, M. J.; Yoon, M.-H.; Facchetti, A.; Marks, T. J.; Wasielewski, M. R. *Angew. Chem. Int. Ed.* **2004**, *43*, 6363−6366. (d) Yoon, M.-H.; DiBenedetto, S.; Facchetti, A.; Marks, T. J. *J. Am. Chem. Soc.* **2005**, *127*, 1348−1349. (e) Letizia, J. A.; Facchetti, A.; Stern, C. L.; Ratner, M. A.; Marks, T. J. *J. Am. Chem. Soc.* **2005**, *127*, 13476−14477.
(17) (a) Facchetti, A.; Wang, A.; Marks, T. J. *Polym. Mater. Sci. Eng.* **2000**, *83*, 290. (b) Garnier, F.; Yassar, A.; Hajlaoui, R.; Horowitz, G.; Deloffre, F.; Servet, B.; Ries, S.; Alnot, P. *J. Am. Chem. Soc.* **1993**, *115*, 8716. (c) Visser, G. J.; Heeres, G. J.; Wolters, J.; Vos, A. *Acta Crystallogr., Sect. B* **1968**, *24*, 467. (d) Pyrka, G. J.; Fernando, Q.; Inoue, M. B.; Inoue, M.; Velazquez, E. F. *Acta Crystallogr., Sect. C* **1988**, *44*, 562. (e) Hotta, S.; Waragai, K. *J. Mater. Chem.* **1991**, *1*, 835. (f) Chaloner, P. A.; Gunatunga, S. R.; Hitchcock, P. B. *Acta Crystallogr., Sect. C* **1994**, *50*, 1941. (g) Pelletier, M.; Brisse, F. *Acta Crystallogr., Sect. C* **1994**, *50*, 1942. (h) Horowitz, G.; Bachet, B.; Yassar, A.; Lang, P.; Demanze, F.; Fave, J.-L.; Garnier, F. *Chem. Mater.* **1995**, *7*, 1337. (i) Siegrist, T.; Fleming, R. M.; Haddon, R. C.; Laudise, R. A.; Lovinger, A. J.; Katz, H. E.; Bridenbaugh, P.; Davis, D. D. *J. Mater. Res.* **1995**, *10*, 2170. (j) Barbarella, G.; Zambianchi, M.; Antolini, L.; Folli, U.; Goldoni, F.; Iarossi, D.; Schenetti, L.; Bongini, A. *J. Chem. Soc., Perkin Trans. 2* **1995**, 1869. (k) Fichou, D.; Bachet, B.; Demanze, F.; Billy, I.; Horowitz, G.; Garnier, F. *Adv. Mater.* **1996**, *8*, 500. (l) Siegrist, T.; Kloc, C.; Laudise, R. A.; Katz, H. E.; Haddon, R. C. *Adv. Mater.* **1998**, *10*, 379.
(18) Antolini, L.; Horowitz, G.; Kouki, F.; Garnier, F. *Adv. Mater.* **1998**, *10*, 382.
(19) (a) DiCesare, N.; Belletete, M.; Marrano, C.; Leclerc, M.; Durocher, G. *J. Phys. Chem. A* **1999**, *103*, 795. (b) DiCesare, N.; Belletete, M.; Garcia, E. R.; Leclerc, M.; Durocher, G. *J. Phys. Chem. A* **1999**, *103*, 3864. (c) DiCesare, N.; Belletete, M.; Leclerc, M.; Durocher, G. *J. Phys. Chem. A* **1999**, *103*, 803. (d) Tedesco, E.; Della Salla, F.; Favaretto, L.; Barbarella, G.; Albesa-Jove, D.; Pisignano, D.; Gigli, G.; Cingolani, R.; Harris, K. D. M. *J. Am. Chem. Soc.* **2003**, *125*, 12277.
(20) (a) Lin, B. C.; Cheng, C. P.; Lao, Z. P. M. *J. Phys. Chem. A* **2003**, *107*, 5241. (b) Malagoli, M.; Brédas, J. L. *Chem. Phys. Lett.* **2000**, *327*, 13. (c) Sakanoue, K.; Motoda, M.; Sugimoto, M.; Sakaki, S. *J. Phys. Chem. A* **1999**, *103*, 5551.
(21) (a) Blomgren, F.; Larsson, S. *Theor. Chem. Acc.* **2003**, *110*, 165. (b) Siriwong, K.; Voityuk, A. A.; Newton, M. D.; Rosch, N. *J. Phys. Chem. B* **2003**, *107*, 2595. (c) Blomgren, F.; Larsson, S.; Nelsen, S. F. *J. Comput. Chem.* **2001**, *22*, 655. (d) Nelsen, S. F.; Blomgren, F. *J. Org. Chem.* **2001**, *66*, 6551. (e) Klimkans, A.; Larsson, S. *Int. J. Quantum Chem.* **2000**, *77*, 211. (f) Nelsen, S. F.; Trieber, D. A.; Nagy, M. A.; Konradsson, A.; Halfen, D. T.; Splan, K. A.; Pladziewicz, J. R. *J. Am. Chem. Soc.* **2000**, *122*, 5940. (g) Nelsen, S. F.; Ismagilov, R. F.; Gentile, K. E.; Nagy, M. A.; Tran, H. Q.; Qu, Q.; Halfen, D. T.; Odegard, A. L.; Pladziewicz, J. R. *J. Am. Chem. Soc.* **1998**, *120*, 8230. (h) Jakobsen, S.; Mikkelsen, K. V.; Pedersen, S. U. *J. Phys. Chem.* **1996**, *100*, 7411. (i) Klimkans, A.; Larsson, S. *Chem. Phys.* **1994**, *189*, 25. (j) Todd, M. D.; Mikkelsen, K. V. *Inorg. Chim. Acta* **1994**, *226*, 237.

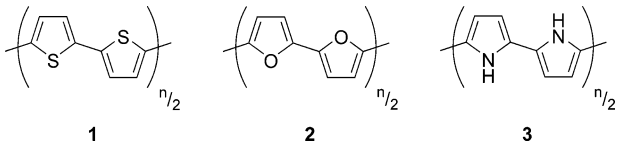

1 2 3

Figure 1. Heterocyclic oligomers investigated, including oligothiophenes **1**, oligofurans **2**, and oligopyrroles **3** of varying dimensions ($n = 2-4$).

(Figure 1), including oligothiophenes, oligofurans, and oligopyrroles. These particular species were chosen both for their diverse structural variations and because of existing experimental and theoretical databases.[22] We employ first-principles calculations (DFT and MP2) to assess both the electronic structures (orbital splittings) and relative packing energetics of these systems, to gain understanding not only of charge transport anisotropy but also of the relative stability of various crystallization arrangements. Unlike band structure calculations, which determine the electronic/energetic nature of one particular crystal structure unit cell, we instead systematically vary the important supramolecular structural parameters to better define the properties of the many different intermolecular packing motifs by examining the underlying molecular pair arrangements.

We show here, for a representative series of oligoheterocycles, that the HOMO and LUMO bandwidths are generally of similar magnitude and that considerable bandwidth anisotropy exists. Analysis of the relative energies of the various possible oligoheterocycle intermolecular packing arrangements indicates that, for separations near those observed experimentally, cofacial or coplanar arrangements exhibit large repulsive interactions and that considerable stabilization exists for *tilted π-stacking* or *slipped (herringbone) π-stacking*, due primarily to electrostatic interactions. Moreover, oligoheterocycle tilted packings exhibit nearly an order of magnitude greater orbital overlap than the corresponding cofacial arrangements at identical center-to-center intermolecular spacings. Furthermore, oligoheterocycle tilted packing motifs exhibit hole and electron bandwidths within 33−50% of those for cofacial stacking at the same smallest intermolecular contact distances, but are significantly more stable energetically. Computed charge-transfer rates, in cofacial, herringbone, and tilted configurations, argue that many of the intrinsic mobility trends observed in these materials are dominated by trends in internal reorganization energies and that

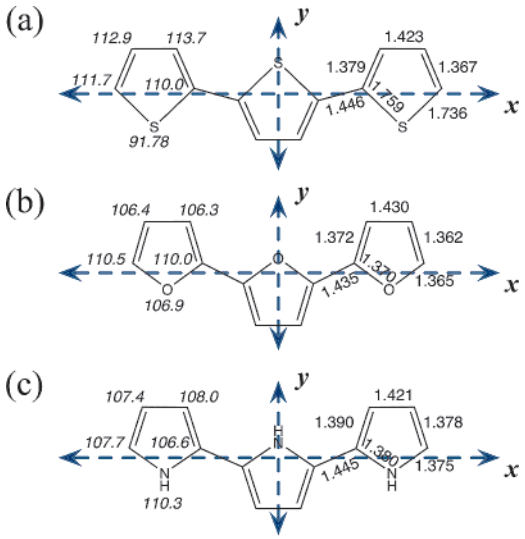

Figure 2. Geometries and standard reference frames for oligomers studied, including (a) terthiophene, (b) terfuran, and (c) terpyrrole. Dashed lines indicate *x* and *y* Cartesian axes for the standard reference frame with the origin at the geometric center of all oligomers and the molecules centered through the *xy*-plane. Numbers indicate B3LYP-optimized geometric parameters, including bond lengths (in Å) in Roman text, and bond angles (in °) in italics.

intrinsic hole and electron mobilities should generally be comparable.[25]

This work identifies several key trends in current generation organic semiconducting materials, including (1) a detailed comparison of the electron and hole bandwidths, which demonstrates that the paucity of *n*-type organic conductive materials is *not due to a small electron bandwidth* (and thus low *n*-type charge mobility), (2) computed overall intrinsic charge-transfer rates for electron and hole transport, *are essentially equal*, except in the slipped-stack direction, where hole transport decreases significantly, and (3) since solid-state structural information is not available for many materials of interest, such as oligofurans and oligopyrroles, a methodological framework is presented for analyzing intermolecular charge transfer between novel molecules without crystal structural constraints.

II. Computational Methods

After full geometry optimizations of the oligothiophene, oligofuran, and oligopyrrole molecular structures were performed using the Q-Chem 2.0 program[26] with the B3LYP hybrid density functional[27] and the 6-31G* basis set, the oligomers were translated into a standard frame of reference with the origin at the molecular geometric center and the *x*-axis along the oligomer long axis (e.g., Figure 2 for the trimers). The optimized molecular geometries tended toward a relatively flat conformation, with the plane of the molecule largely in the *xy*-plane. Inter-ring dihedral angles for oligothiophenes averaged ∼160°, while for oligofurans and oligopyrroles, inter-ring dihedral angles were ∼180° (in line with typical dihedral angles observed in oligothiophene crystal structures).[16−18]

(22) (a) Seixas de Melo, J.; Elisei, F.; Gartner, C.; Gaetano Aloisi, G.; Becker, R. S. *J. Phys. Chem. A* **2000**, *104*, 6907. (b) Fichou, D. *Handbook of Oligo- and Polythiophenes*; Wiley-VCH: Weinheim, New York, 1999. (c) Cornil, J.; Beljonne, D.; Brédas, J. L. *Electronic Materials: The Oligomer Approach*; Wiley-VCH: Weinheim, Germany, 1998; p 432. (d) Bäuerle, P. In *Electronic Materials: The Oligomer Approach*; Müllen, K., Egner, G., Eds.; Wiley-VCH: Weinheim, Germany, 1998; p 105. (e) Groenendaal, L.; Meijer, E. W.; Vekemans, J. A. J. M. In *Electronic Materials: The Oligomer Approach*; Müllen, K., Egner, G., Eds.; Wiley-VCH: Weinheim, Germany, 1998; p 235. (f) McCullough, R. D. *Adv. Mater.* **1998**, *10*, 93. (g) Glenis, S.; Benz, M.; Legoff, E.; Schindler, J. L.; Kannewurf, C. R.; Kanatzidis, M. G. *J. Am. Chem. Soc.* **1993**, *115*, 12519. (h) Kauffmann, T.; Lexy, H. *Chem. Ber.* **1981**, *114*, 3667.
(23) (a) Gorman, C. B.; Marder, S. R. *Chem. Mater.* **1995**, *7*, 215. (b) Meyers, F.; Marder, S. R.; Pierce, B. M.; Brédas, J. L. *J. Am. Chem. Soc.* **1994**, *116*, 10703. (c) Bourhill, G.; Brédas, J.-L.; Cheng, L.-T.; Marder, S. R.; Meyers, F.; Perry, J. W.; Tiemann, B. G. *J. Am. Chem. Soc.* **1994**, *116*, 2619. (d) Marder, S. R.; Perry, J. W.; Bourhill, G.; Gorman, C. B.; Tiemann, B. G.; Mansour, K. *Science* **1993**, *261*, 186. (e) Marder, S. R.; Perry, J. W.; Tiemann, B. G.; Gorman, C. B.; Gilmour, S.; Biddle, S. L.; Bourhill, G. *J. Am. Chem. Soc.* **1993**, *115*, 2524. (f) Cui, C. X.; Kertesz, M.; Jiang, Y. *J. Phys. Chem.* **1990**, *94*, 5172. (g) Lee, Y. S.; Kertesz, M. *J. Chem. Phys.* **1988**, *88*, 2609. (h) Hutchison, G. R.; Ratner, M. A.; Marks, T. J. *J. Phys. Chem. B* **2005**, *109*, 3126.
(24) Hutchison, G. R.; Zhao, Y. J.; Delley, B.; Freeman, A. J.; Ratner, M. A.; Marks, T. J. *Phys. Rev. B* **2003**, *68*, 035204.
(25) Communicated in part at: (a) Excited State Processes in Electronic and Bio-Nanomaterials, Los Alamos, August 11−16, 2003. (b) ACS Prospectives Symposium "Organic Thin Film Electronics", Miami, Jan. 25−28, 2004. (c) The 227th National Meeting of the ACS, Anaheim CA.; Facchetti, A.; Hutchison, G.; Yoon, M.-H.; Letizia, J.; Ratner, M. A.; Marks, T. J. Polymer Preprints, 2004, 45, 185−186. (d) Sixth International Symposium on Functional π-Electron Systems, Ithaca, NY, June 14−18, 2004.
(26) Kong, J. et al. *J. Comput. Chem.* **2000**, *21*, 1532.
(27) (a) Becke, A. D. *J. Chem. Phys.* **1993**, *98*, 5648. (b) Lee, C.; Yang, W.; Parr, R. G. *Phys. Rev. B* **1988**, *37*, 785.

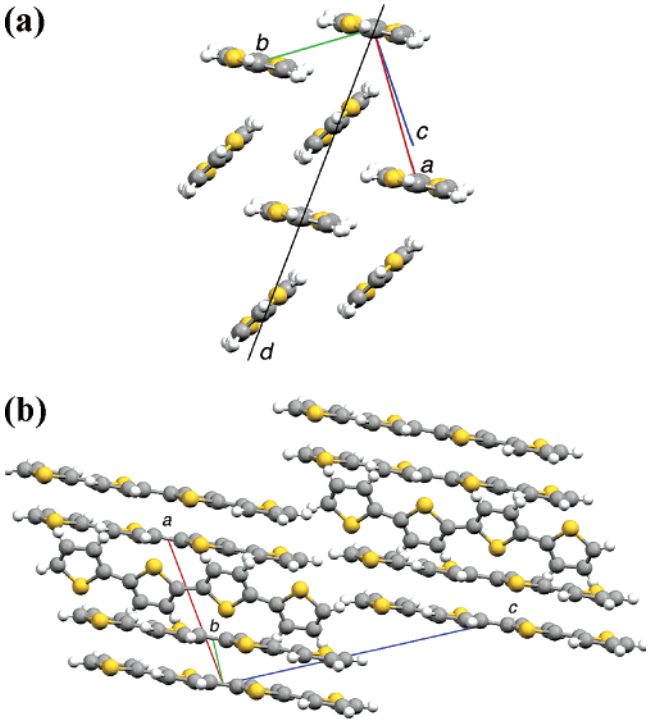

Figure 3. Experimental single-crystal packing of tetrathiophene (ref 16), (a) projection in the *ab*-plane, showing a π-herringbone stacking (slipped-stacked) motif extending along the *b*-axis, and along the diagonal "*d*"-axis between herringbone stacks as tilted π-stacks; (b) projection in the *ac*-plane showing the relative orientations of the molecular planes.

While experimental single-crystal structures are unknown for oligofurans and oligopyrroles, it is reasonable to assume initially that they adopt structures similar to those observed in oligothiophene crystal structures[16−18] (e.g., Figure 3 for tetrathiophene[18]). In particular, oligothiophenes crystallize in herringbone motifs[16−18] (e.g., extending along the *b*-axis as shown in Figure 3) rather than in cofacial π-stacks. Across the herringbone stacks (e.g., extending along the "*d*" diagonal axis in Figure 3) are tilted π-stacks. The herringbone and tilted motifs resemble the slipped-stacking and T-shaped motifs observed in benzene π-dimers (viewed along the ring planes below).[28,29] Tilted π-stacks are also observed in gas-phase pyrrole dimers, with tilt angles from experiment of 55.4°[30] and computational modeling of ∼60−70°.[31] However, to examine a more complete range of potential intermolecular packing arrangements, other motifs must be considered.

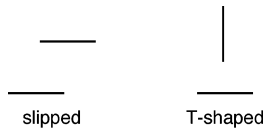

Intermolecular packing arrangements can be most simply described in terms of direct translations along a Cartesian direction, using the frame in Figure 2. One molecule remains centered at the origin, and a second is placed at a given center-to-center distance along one axis, as illustrated in Figure 4. The separations between two coplanar molecules are modulated by translations along the *x*- or *y*-axes, while those between cofacially π-stacked molecules are modulated by *z*-axis translations. In addition, one oligomer can be "flipped" about the

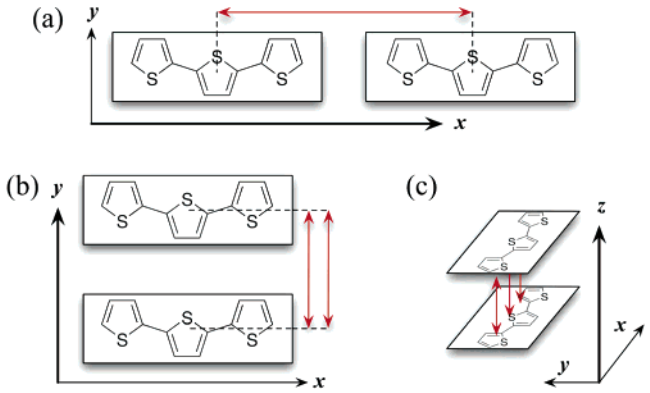

Figure 4. Diagram of various dimer arrangements for oligothiophenes, illustrating intermolecular interactions along the (a) *x*, (b) *y*, and (c) *z* Cartesian axes, as defined by the frame of reference in Figure 2. Interactions along the *x*- and *y*-axes involve two molecules coplanar in the *xy*-plane, while the *z*-axis represents a cofacial π-stack. Two orientations between the molecules exist, an "eclipsed" orientation (above), with the same heteroatom orientation in both molecules, and the "inverted" orientation involving a 180° rotation of one molecule about the longitudinal molecular axis (parallel to the *x*-axis).

longitudinal molecular axis (parallel to the *x*-axis) to yield an "inverted" rather than an "eclipsed" orientation. A tilted π-stack can be derived from a translation along the *z*-axis, followed by a rotation about the longitudinal molecular (or *x* Cartesian) axis, as illustrated in Figure 5, with the eclipsed and inverted cofacial stack orientations being the two endpoints of this operation, at tilt angles of 0 and 180°, respectively. A slipped π-stack to model the herringbone packings can be derived from a translation along both the *z*- and *y*-axes, as illustrated in Figure 6.

To analyze as wide a range of intermolecular motifs as possible, the range used for the basic Cartesian translations started from approximately close-packing at van der Waals contacts between molecules and extended several angstroms along each axis (i.e., center-to-center displacements along *x*: 11.0−16.0 Å for dimers, 15.0−20.0 Å for trimers, 18.0−25.0 Å for tetramers; along *y*: 7.0−12.0 Å; along *z*: 3.0−9.5 Å). For tilted π-stacks, the center-to-center displacement in several experimental single-crystal structures is approximately 5.0 Å,[16−18,32] so three *z*-axis displacements were studied in detail: 5.0, 6.5, and 8.0 Å, varying the tilt angle from 0 to 180° in 15° increments. For slipped π-stacks, the experimental crystal structures exhibit displacement along the *y*-axis (i.e., the short molecular axis) of approximately one full molecular width (∼4.8 Å), so first the *z*-axis displacement was varied from 3 to 4.0 Å at a fixed 4.84 Å *y*-axis center-to-center distance (Figure 6a), and then the *y*-axis displacement was varied from 4.5 to 5.5 Å at a fixed 3.1 Å *z*-axis center-to-center distance (Figure 6b)—the distance in the tetrathiophene crystal structure of Figure 3.[18] The large number of spatial orientations examined and consideration of different oligoheterocycles and differing oligomer lengths allows statistical analysis of the results to minimize the effects of small random errors and to provide greater confidence in the predicted consequences of each principal structural modification.

The electronic structure of each molecular pair was computed using both B3LYP and ab initio Møller−Plessett 2 (MP2) methods and the 6-31G* or 6-31+G* basis sets,[33] converging to accuracies of better than 10^{-6} and 10^{-7} hartree for B3LYP and MP2, respectively, and using 10^{-9} and 10^{-10} hartree criteria for neglect of two-electron integrals, respectively, to achieve improved numerical accuracy. While current

(28) Tsuzuki, S.; Uchimaru, T.; Sugawara, K.-i.; Mikami, M. *J. Chem. Phys.* **2002**, *117*, 11216.
(29) Hunter, C. A.; Lawson, K. R.; Perkins, J.; Urch, C. J. *J. Chem. Soc., Perkin Trans. 2* **2001**, 651.
(30) Columberg, G.; Bauder, A. *J. Chem. Phys.* **1997**, *106*, 504.
(31) (a) Park, H.; Lee, S. *Chem. Phys. Lett.* **1999**, *301*, 487. (b) Stefov, V.; Pejov, L.; Soptrajanov, B. *J. Mol. Struct.* **2003**, *649*, 231.
(32) Facchetti, A.; Yoon, M.-H.; Hutchison, G. R.; Stern, C. L.; Ratner, M. A.; Marks, T. J. *J. Am. Chem. Soc.* **2004**, *126*, 13480.
(33) Except where indicated, calculations use the 6-31G* basis set. We recomputed potential energy curves and surfaces with the more accurate 6-31+G* basis set and counterpoise corrections, though the increased basis set has no effect on the computed orbital energy levels, as illustrated in Figure 8.

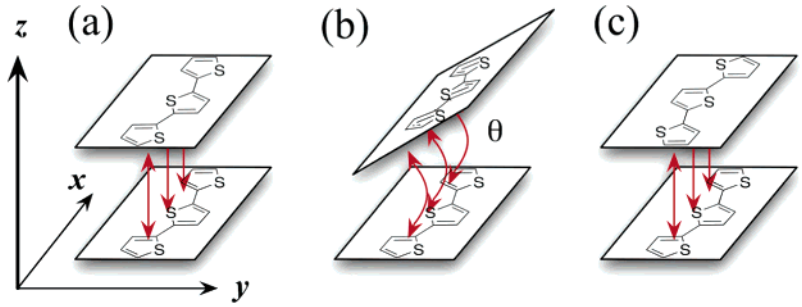

Figure 5. Illustrations of the tilted π-stacking arrangement of oligomers, representing displacements along the *z*-axis and rotations along the longitudinal molecular axis (*x*-axis) and resembling the *d*-axis in Figure 3. Note that the eclipsed orientation represents a tilt angle of (a) 0°, which can be varied (b) all the way to the inverted orientation, which represents a tilt angle of 180° (c).

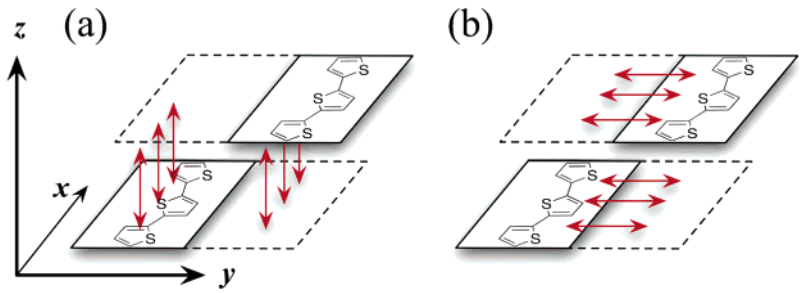

Figure 6. Illustrations of the slipped π-stacked arrangement of oligomers, representing displacements along the *z*-axis followed by translation along the *y*-axis and modeling the herringbone motif parallel to the *b*-axis in Figure 3. Note that for this work, only variations in (a) the *z*-axis displacement (i.e., between herringbone planes), and (b) the *y*-axis displacement are analyzed independently.

density functional methods are known to give excellent predictions of bandwidths in solid-state materials,[34] they describe weak interactions poorly.[35,36] Conversely, the MP2 method has gained wide acceptance for treating correlation and dispersion interactions reasonably well,[36] including the weak electrostatic and dispersive energetic interactions between organic π-dimers, such as benzene and thiophene,[28,37−39] but Hartree−Fock orbital energies (i.e., from the MP2 calculations here) have been less employed for bandwidths or orbital overlap.[40] Hence, correlation of electronic structures and relative energies computed by each method should help ensure accurate treatment of both properties.

Internal reorganization energies between relaxed neutral and anion geometries were calculated using B3LYP, which has been shown to give λ values in excellent agreement with those measured experimentally for aromatic cations.[41] Analogous oligoheterocycle cation λ values were calculated previously.[13]

All statistical analyses, including multifactor analysis of variance (ANOVA), were performed with the R statistical package, version 1.8.0,[42] as described below. Molecular orbital and electrostatic potential surfaces were plotted using Spartan 02.[26,43]

III. Results and Discussion

We first consider the accuracy of the computational methods employed, including comparisons with previous work. We then discuss the statistical analysis of the results and the correlations thereby suggested for the dependence of HOMO and LUMO splittings on relative intermolecular orientations, heteroatom identity, oligomer lengths, the tilt angle for *z*-axis/π-stacking, and translational effects for slipped π-stacks. These results are then used to compare computed hole transfer rates for oligothiophenes, oligofurans, and oligopyrroles, and we conclude by discussing the consequences for design of both *p*-type and *n*-type electrically conductive oligoheterocycles.

A. Comparison of MP2 and DFT/B3LYP Methods and Basis Set Effects. Density functional methods have long been used to predict accurate bandwidths in solid-state materials, and the B3LYP functional has proven to be accurate for calculating ionization potentials,[44] electron affinities,[44,45] HOMO/LUMO gaps,[46] and molecular geometries.[47] However, it is also known to describe weak interactions poorly, including van der Waals and $\pi-\pi$ interactions.[35,36] Since the intermolecular interactions

(34) Delley, B. *J. Chem. Phys.* **2000**, *113*, 7756.
(35) (a) Wu, Q.; Yang, W. *J. Chem. Phys.* **2002**, *116*, 515. (b) Wu, X.; Vargas, M. C.; Nayak, S.; Lotrich, V.; Scoles, G. *J. Chem. Phys.* **2001**, *115*, 8748. (c) Kohn, W.; Meir, Y.; Makarov, D. E. *Phys. Rev. Lett.* **1998**, *80*, 4153. (d) Zhang, Y.; Pan, W.; Yang, W. *J. Chem. Phys.* **1997**, *107*, 7921. (e) Lundqvist, B. I.; Andersson, Y.; Shao, H.; Chan, S.; Langreth, D. C. *Int. J. Quantum Chem.* **1995**, *56*, 247.
(36) Kurita, N.; Sekino, H. *Chem. Phys. Lett.* **2001**, *348*, 139.
(37) (a) Reyes, A.; Tlenkopatchev, M. A.; Fomina, L.; Guadarrama, P.; Fomine, S. *J. Phys. Chem. A* **2003**, *107*, 7027. (b) Huh, S. B.; Lee, J. S. *J. Chem. Phys.* **2003**, *118*, 3035. (c) Sinnokrot, M. O.; Valeev, E. F.; Sherrill, C. D. *J. Am. Chem. Soc.* **2002**, *124*, 10887. (d) Lee, N. K.; Park, S.; Kim, S. K. *J. Chem. Phys.* **2002**, *116*, 7910. (e) Lee, N. K.; Park, S.; Kim, S. K. *J. Chem. Phys.* **2002**, *116*, 7902.
(38) (a) Tsuzuki, S.; Honda, K.; Azumi, R. *J. Am. Chem. Soc.* **2002**, *124*, 12200. (b) Tsuzuki, S.; Honda, K.; Uchimaru, T.; Mikami, M.; Tanabe, K. *J. Am. Chem. Soc.* **2002**, *124*, 104.
(39) Tsuzuki, S.; Uchimaru, T.; Matsumura, K.; Mikami, M.; Tanabe, K. *Chem. Phys. Lett.* **2000**, *319*, 547.
(40) Suhai, S. *Int. J. Quantum Chem.* **1992**, *42*, 193.
(41) (a) Gruhn, N. E.; da Silva, D. A.; Bill, T. G.; Malagoli, M.; Coropceanu, V.; Kahn, A.; Brédas, J. L. *J. Am. Chem. Soc.* **2002**, *124*, 7918. (b) Amashukeli, X.; Winkler, J. R.; Gray, H. B.; Gruhn, N. E.; Lichtenberger, D. L. *J. Phys. Chem. A* **2002**, *106*, 7593.
(42) Ihaka, R.; Gentleman, R. *J. Comput. Graph. Statist.* **1996**, *5*, 299.
(43) *Spartan 02*; Wavefunction, Inc.: Irvine, CA, 2000.
(44) Zhan, C. G.; Nichols, J. A.; Dixon, D. A. *J. Phys. Chem. A* **2003**, *107*, 4184.
(45) (a) Rienstra-Kiracofe, J. C.; Tschumper, G. S.; Schaefer, H. F.; Nandi, S.; Ellison, G. B. *Chem. Rev.* **2002**, *102*, 231. (b) Rienstra-Kiracofe, J. C.; Barden, C. J.; Brown, S. T.; Schaefer, H. F. *J. Phys. Chem. A* **2001**, *105*, 524. (c) de Oliveira, G.; Martin, J. M. L.; de Proft, F.; Geerlings, P. *Phys. Rev. A* **1999**, *60*, 1034. (d) Curtiss, L. A.; Redfern, P. C.; Raghavachari, K.; Pople, J. A. *J. Chem. Phys.* **1998**, *109*, 42. (e) DeProft, F.; Geerlings, P. *J. Chem. Phys.* **1997**, *106*, 3270.
(46) (a) Muscat, J.; Wander, A.; Harrison, N. M. *Chem. Phys. Lett.* **2001**, *342*, 397. (b) Hutchison, G. R. Theoretical Studies of Optics and Charge Transport in Organic Conducting Oligomers and Polymers: Rational Design of Improved Transparent and Conducting Polymers. Ph.D. Dissertation, Northwestern University, Evanston, Illinois, 2004.
(47) (a) Hehre, W. J. *A Guide to Molecular Mechanics and Quantum Chemical Calculations*; Wavefunction, Inc.: Irvine, CA, 2003. (b) Curtiss, L. A.; Redfern, P. C.; Raghavachari, K.; Pople, J. A. *J. Chem. Phys.* **2001**, *114*, 108. (c) Bauschlicher, C. W. *Chem. Phys. Lett.* **1995**, *246*, 40.

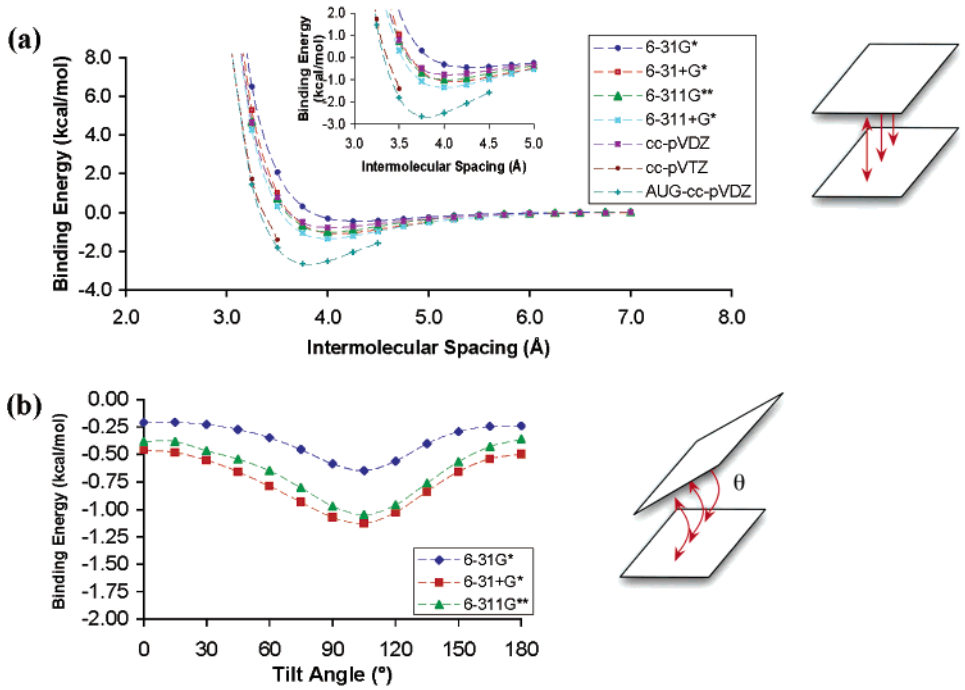

Figure 7. Comparison of basis set effects (using a logarithmic *y*-axis) for counterpoise-corrected MP2 calculations on π-stacked thiophene pairs for (a) changes in intermolecular spacing and for (b) dimers having various interplanar tilt angles, θ, with a 5.0 Å center-to-center spacing. Note that while the magnitudes of the energetic maxima and minima are somewhat basis-set-dependent, as expected, the shape of the curves and, in particular, the extremum geometries, are not substantially basis-set-dependent.

here are primarily $\pi-\pi$ stacking and van der Waals in nature, second-order Møller−Plesset (MP2) ab initio calculations (useful for treating dispersion and weak interactions[28,37−39]) were also performed for comparison. Since Hartree−Fock (HF) orbital energies (i.e., from the MP2 results here) have been used less for computing bandwidths,[40] careful comparison of the results of the two methods should prove to be informative as to the reliability of each.

Since treatment of dispersion effects, for example, in aromatic π-systems such as benzene, is basis-set dependent,[38,39] test counterpoise-corrected MP2 calculations were performed with multiple basis sets on a thiophene cofacial π-stacked pair (Figure 7). In agreement with previous studies of π-stacked dimers,[38] while the relative energies differ with different basis sets, the positions/geometries of the minima/maxima are largely independent of basis set.[48] Similarly, the HOMO and LUMO orbital splittings computed here are largely independent of basis set (Figure 8) beyond the minimal STO-3G basis, except at large intermolecular separation, where the splittings are small in magnitude in any case. Since binding energies are substantially basis-set dependent, even the counterpoise-corrected binding energies presented here should be considered as only semi-quantitative trends. Figure 9 shows a comparison of the counterpoise-corrected binding energies of the dimers of trimeric oligoheterocycles **1**−**3** with relative displacements along the *x*-, *y*-, and *z*-axes (Figure 4) for both B3LYP and MP2 computational methods. The DFT method sometimes yields artifacts in the relative energies, particularly for displacements along *y* (smaller energy "bumps" are present in the *x* and *z*

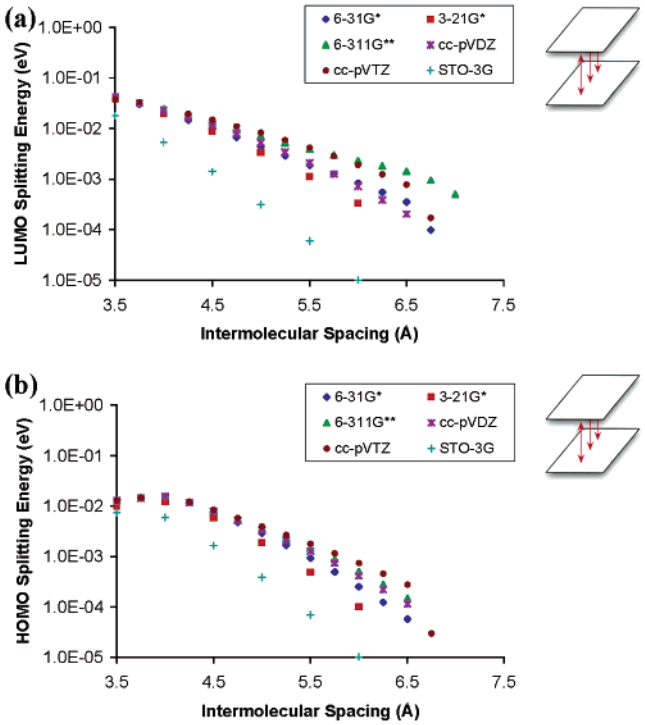

Figure 8. Basis set dependence of HF-computed orbital splitting energies (using a logarithmic *y*-axis) for (a) LUMO and (b) HOMO orbitals of eclipsed π-stacked bithiophene pairs. Note that any basis set dependence of the orbital splittings over the distances considered here are small in absolute magnitude (except for the minimal basis set, STO-3G) and only occur at large intermolecular spacings.

displacements as well, but are obscured by the scale of the figure). Figure S1 compares the computed HF and B3LYP dimer orbital energy splittings for both HOMO and LUMO orbitals across all three oligomer series and all three oligomer lengths considered ($n = 2-4$) in the π-stacking direction. While

(48) In general, this is true only if basis set superposition errors (BSSE) are taken into account, for example, with counterpoise corrections. In these systems, as discussed below, the counterpoise-corrected binding energies do not show substantially different curves or extrema than the uncorrected relative energy curves.

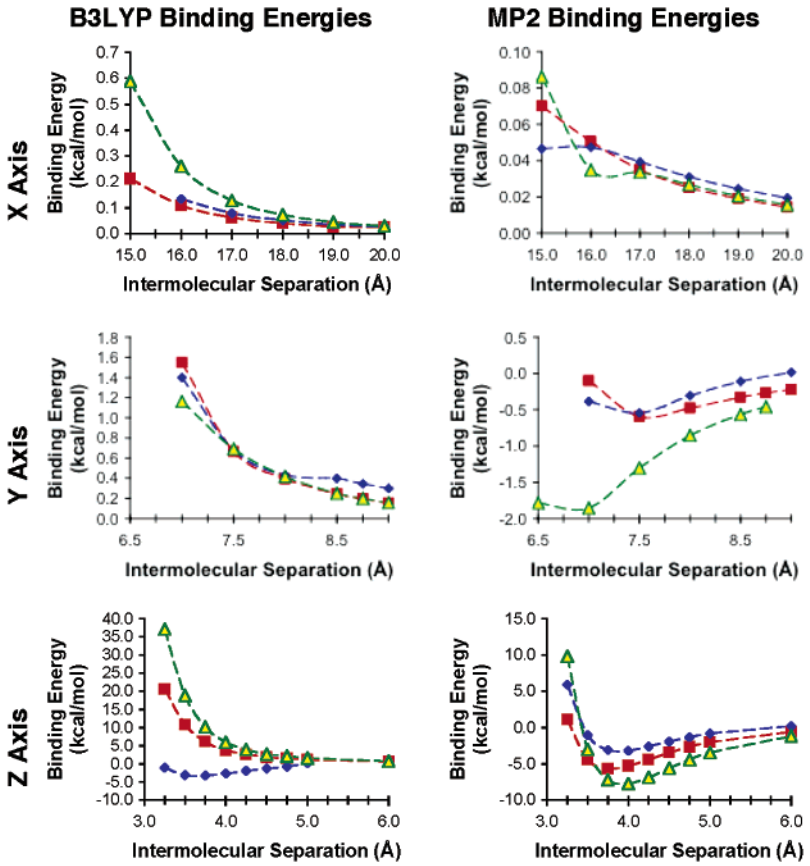

Figure 9. Counterpoise-corrected binding energies of dimers as a function of the center-to-center intermolecular spacing along the axes indicated (Figure 4) for terthiophene (△), terfuran (■), and terpyrrole (◆) having the eclipsed orientation. Note that for B3LYP/6-31+G* repulsive interactions are generally observed even out to large intermolecular separations, while MP2/6-31+G* calculation demonstrates binding for *y* and *z* Cartesian axes.

computed orbital splitting energies are greater for B3LYP than for HF, the two methods show high correlation ($R^2 = 0.996$ and 0.991 for HOMO and LUMO splittings, respectively). This observation is surprising, considering that the HF-computed LUMOs are consistently too diffuse due to neglect of correlation, and DFT functionals suffer from approximations in the exchange−correlation functional and are known to poorly describe unoccupied states. Lower-level DFT calculations on organic conjugated materials, however, have consistently demonstrated comparable bandwidths to those computed by high-level DFT quasiparticle methods, even if the HOMO−LUMO gap differs.[49,50]

Consequently, since the HF-derived orbital splittings are similar to the B3LYP splittings and the MP2-computed relative energy profiles are more reliable, the present discussion generally focuses on the MP2 results, unless otherwise indicated. The results of the DFT calculations are, in general, qualitatively very similar.

B. Influence of Intermolecular Orientation, Heteroatom, and Oligomer Length. As mentioned above, Figure 9 shows the dimer potential energy behavior for displacement along the three Cartesian axes (Figure 4) for three triheterocycles; these indicate purely repulsive interactions for all heteroatoms, oligomer lengths, and eclipsed/inverted orientations. However, with the exception of the *z*-axis cofacial π-stacking, the magnitudes of the energetic changes are modest and in actual crystal structures may be balanced by the overall free energy of packing. The consequences of the *x*-axis and *y*-axis displacements primarily reflect the differences in the structures of the three trimers considered—the trithiophene is longer than the tripyrrole or trifuran (12.42 Å versus 11.42 and 11.07 Å, respectively), while the results of the *z*-axis displacements correlate with the van der Waals radii of the heteroatoms involved (1.70, 1.85, and 2.0 Å for O, N, and S, respectively).[51] Even for *z*-axis displacement, beyond a separation of 4.0 Å, the relative computed energies in general fall by only ∼2−6 kcal/mol out to 9.50 Å intermolecular separation. Since the magnitudes of these binding energies are highly basis-set-dependent and thus the results are more useful for discerning qualitative/semiquantitative trends, the results have not been tabulated, but representative trends are presented (e.g., in Figure 9) and discussed where appropriate below. These same general trends were also observed for the homologous bi- and tetraheterocycles.

Before comparing orbital splitting energies, it is useful to consider the spatial dependence of the computed HOMO and LUMO contour surfaces in the reference frame defined above (Figure 2). Figure 10 shows the DFT-computed HOMO and

(49) (a) van der Horst, J. W.; Bobbert, P. A.; Michels, M. A. J.; Brocks, G.; Kelly, P. J. *Synth. Met.* **1999**, *101*, 333. (b) van der Horst, J. W.; Bobbert, P. A.; de Jong, P. H. L.; Michels, M. A. J.; Brocks, G.; Kelly, P. J. *Phys. Rev. B* **2000**, *61*, 15817. (c) Rohlfing, M.; Louie, S. G. *Phys. Rev. Lett.* **1999**, *82*, 1959. (d) Rohlfing, M.; Tiago, M. L.; Louie, S. G. *Synth. Met.* **2001**, *116*, 101. (e) Ferretti, A.; Ruini, A.; Molinari, E.; Caldas, M. J. *Phys. Rev. Lett.* **2003**, *90*, 086401/1. (f) Bussi, G.; Ferretti, A.; Ruini, A.; Caldas, M. J.; Molinari, E. *Adv. Solid State Phys.* **2003**, *43*, 313. (g) Ruini, A.; Bussi, G.; Ferretti, A.; Caldas, M. J.; Molinari, E. *Synth. Met.* **2003**, *139*, 755.

(50) (a) Tiago, M. L.; Northrup, J. E.; Louie, S. G. *Phys. Rev. B* **2003**, *67*, 115212/1. (b) Ferretti, A.; Ruini, A.; Bussi, G.; Molinari, E.; Caldas, M. J. *Phys. Rev. B* **2004**, *69*, 205205/1.

(51) *Handbook of Chemistry and Physics*; CRC Press: Boca Raton, FL, 1995.

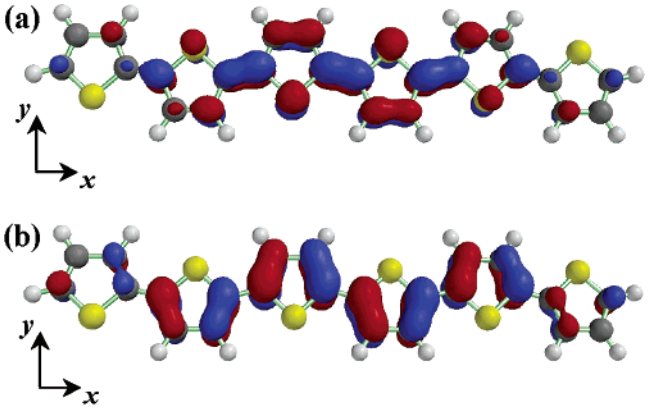

Figure 10. Orbital contour maps of the (a) LUMO and (b) HOMO for sexithiophene in the same reference frame as in Figure 2. Although sexithiophene is plotted here, the patterns are similar in other oligothiophenes. Principal orbital populations are depicted in red and blue.

LUMO surfaces for sexithiophene, which are representative of the motifs for all oligoheterocycles considered here. The HOMOs are principally composed of ring C=C bonds, aligned predominantly along the *y*-axis. The LUMOs are principally composed of inter-ring formal C−C single bonds, the heteroatoms, and formally single C−C intra-ring bonds, all aligned predominantly along the *x*-axis.

Figure 11 shows the computed HOMO and LUMO energy splittings as a function of intermolecular separation for all three tetramers and for displacements in all three Cartesian directions. Since this interaction reflects the overlap of the two molecular orbitals, the computed splittings (*s*) are expected to exhibit inverse exponential dependence on the intermolecular center-to-center distance (*d*). Indeed, the data can be fit by:

$$\ln(s) = C_0 + C_1 d \qquad (3)$$

where C_0 and C_1 are fitting parameters. Due to potential size-consistency and numerical accuracy issues inherent in the computational method, statistical fittings were performed only on a subset of the data, namely, at the smaller separations with greater orbital overlap (*x*-axis, 11.0−13.0, 15.0−17.0, and 18.0−20.0 Å for dimers through tetramers, respectively; *y*-axis, 7.0−9.5 Å; and *z*-axis, 3.0−7.0 Å). Greater overlap values should lead to proportionally smaller errors and hence to more accurate fits. All fits for the MP2-computed HOMO and LUMO splittings are compiled in Table S1, while the B3LYP-computed fits are compiled in Table S2. Several translations along the *x*-axis show poor fits to exponential behavior (i.e., low R^2 values) but, not surprisingly, also have small computed bandwidths (e.g., $< 10^{-2}-10^{-3}$ eV as illustrated in Figure 11) and are unlikely to be major charge-transport pathways.

To gain an overall understanding of the interplay of variables (heteroatom, oligomer length, axis, eclipsed/inverted orientation) in this multidimensional study, we employ multivariate analysis of variance (ANOVA) on the linear regression results. This statistical technique highlights the effect of one particular geometric/structural change on the orbital splittings as represented by the coefficients of the exponential fits and reveals statistically significant correlations for further analysis by

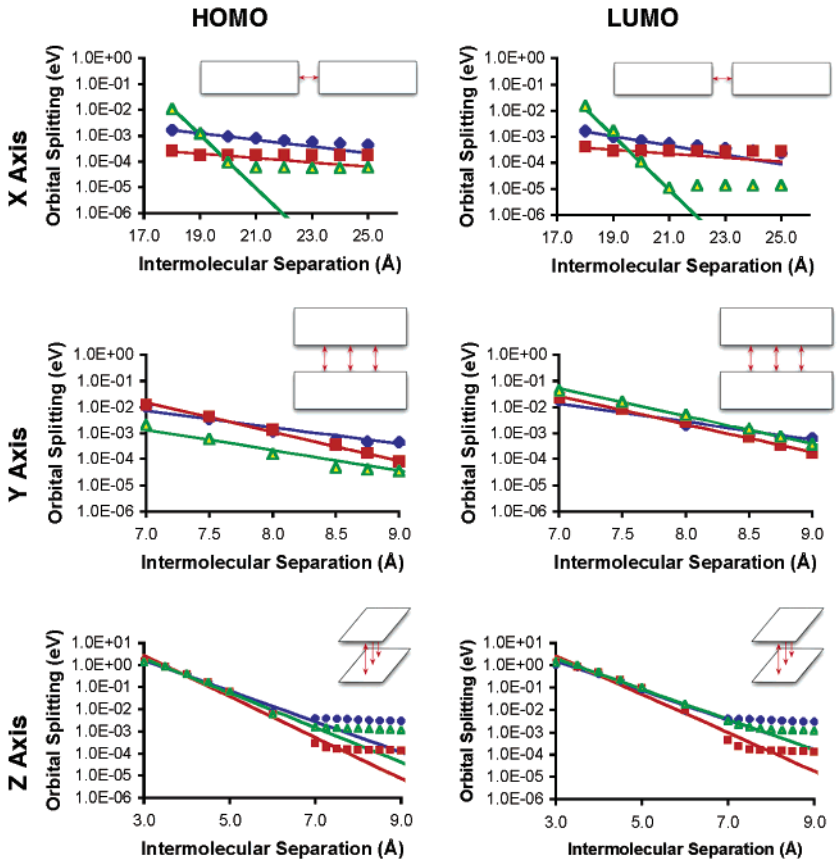

Figure 11. HF-derived HOMO and LUMO level splittings (on a logarithmic scale) as a function of the intermolecular spacing along the specified axis (Figure 4) for tetrathiophene (△), tetrafuran (■), and tetrapyrrole (◆) in eclipsed orientation. Solid lines are the exponential fits given in Table S1. Note that the fits generally underestimate the computed splittings at the largest separations (where the orbital splittings are small in magnitude), but fit more closely for the remaining points.

Table 1. Four-Way ANOVA Analysis of the Principal Factors and Interactions for Computed Oligoheterocycle HOMO and LUMO Orbital Splitting Parameters (C_0, C_1) Using Both HF and DFT/B3LYP Methods from the Data in Table S1[a]

	MP2 (HF)				B3LYP			
	HOMO		LUMO		HOMO		LUMO	
effect	C_0	C_1	C_0	C_1	C_0	C_1	C_0	C_1
Principal Factors								
heteroatom	X	X	X	X	X		X	X
oligomer length (no. of monomers)		X						
orientation						X		
axis	X	X	X	X	X	X	X	X
Interactions (2nd order)								
heteroatom:oligomer length	X				X			
heteroatom:orientation								
heteroatom:axis	X	X	X	X	X	X	X	X
oligomer length:orientation								
oligomer length:axis						X		
orientation:axis					X			
Interactions (3rd order)								
heteroatom:oligomer length:orientation								
heteroatom:oligomer length:axis	X				X			
heteroatom:orientation:axis								
oligomer length:orientation:axis								

[a] Filled cells (X) indicate factors which are statistically significant for that variable with a 95% confidence level. These summarize which factors are important in dictating the response of each variable and whether these effects are independent (i.e., whether 2nd or 3rd order interactions are significant).

comparing whether the groups formed by particular geometric/structural changes have similar or different centroids. The effect of each factor may not be completely independent of other factors. For example, each oligomer has a slightly different geometry, so the oligoheterocycle with greatest splitting in the *x* direction may have the least splitting in the *y* direction because of the greater molecular length. Consequently, the ANOVA results summarized in Table 1 for the HF- and B3LYP-computed orbital splittings consider all potential second- and third-order interactions, which would be important for these nonindependent effects, indicating significant effects as those with confidence levels of 95% or higher. In general, interaction effects represent combinations of pairs, triplets, or other combinations of independent factors, acting as correction factors to the results predicted simply by orthogonal main effects acting alone.[52]

Table 1 suggests that the three most consistently important factors in the computed intermolecular orbital splittings are the heteroatom, the Cartesian displacement axis, and the second-order interaction between the two (these two effects are not independent). The computed splittings in Figure 11 show some dependence on heteroatom, particularly along the *x*- and *y*-axes, which can be explained by structural differences in the three oligoheterocycles. Along the *x* direction (long axis), oligothiophenes exhibit somewhat larger computed orbital splittings. At a center-to-center separation of 18.0 Å along the *x*-axis, the tetrathiophene pairs have a 1.74 Å separation between terminal H atoms (3.73 Å closest C−C distance), while the corresponding oligopyrrole and oligofuran have 2.99 and 3.44 Å H−H separations, respectively. Consequently, decreased overlap is computed for the oligopyrroles and oligofurans. Along the *y*-axis, at 7.0 Å separation between molecular centers, tetrafuran, tetrapyrrole, and tetrathiophene molecular pairs have 2.13, 2.18, and 2.57 Å separations between closest contacts (H-heteroatom), explaining the observed ordering of small HOMO splittings. However, along the *y*-axis, the longer C−S bonds and greater van der Waals radius of S relative to that of O and N leads to greater overlap from the LUMO portion residing on the heteroatom (Figure 10a) and the neighboring molecule.

Table 2. Three-Way ANOVA Analysis of the Principal Factors and Interactions for Computed Oligoheterocycle HOMO and LUMO Orbital Splitting Parameters (C_0, C_1) in the *z*/π-Stacking Axis, Using Both HF and DFT/B3LYP Methods from the Data in Table S1[a]

	MP2 (HF)				B3LYP			
	HOMO		LUMO		HOMO		LUMO	
effect	C_0	C_1	C_0	C_1	C_0	C_1	C_0	C_1
Principal Factors								
heteroatom		X	X	X			X	X
oligomer length (no. of monomers)	X		X	X			X	
orientation	X				X			
Interactions (2nd order)								
heteroatom:oligomer length			X					
heteroatom:orientation								
oligomer length:orientation								
Interactions (3rd order)								
heteroatom:oligomer length:orientation								

[a] Filled cells (X) indicate factors which are statistically significant for that variable with a 95% confidence level. These summarize which factors are important in dictating the response of each variable and whether these effects are independent (i.e., whether 2nd or 3rd order interactions are significant).

The results in Figure 11 indicate that changing intermolecular separation along the *z*-axis/π-stacking direction gives quantitatively similar and large bandwidth changes for *both* HOMOs and LUMOs, but also that the bandwidths are essentially independent of heteroatom. An ANOVA analysis restricted to *z*-axis displacement is summarized in Table 2 and indicates that heteroatom identity, oligomer length, and orientation are all potentially important, but likely function independently since only one potential second- or third-order interaction is significant at the 95% confidence level, suggesting that the different heterocycles scale differently as a function of oligomer length. Small differences do exist, as illustrated in Figure 12, which compares orbital splittings at a fixed separation of 4.0 Å as a function of oligomer length (other separations yield almost identical trends). The computed orbital HOMO splittings for the different oligomers are very similar, and splitting decreases as a function of oligomer length for all three. This is consistent with the HOMO composition; it does not include appreciable heteroatom population, only carbon backbone (Figure 10b). In contrast, as suggested by the contours in Figure 10, the LUMOs exhibit decreased orbital splittings as a function of heteroatom, from thiophene to furan to pyrrole, in order of increasing heterocycle electron density. Furthermore, the decrease in LUMO overlap as a function of oligomer length is greater for oligofurans and oligopyrroles than for oligothiophenes—exactly the sort of interdependence suggested by ANOVA (Table 2).

The decrease in HOMO and LUMO splittings as a function of oligomer length is different from that observed in previous INDO/S calculations on oligothiophenes.[8] That work reported

(52) For more information on multivariate ANOVA or multivariate linear regression techniques used here, see for example: (a) Cobb, G. W. *Introduction to Design and Analysis of Experiments*; Springer: New York, 1998. (b) Box, G. E. P.; Hunter, W. G.; Hunter, J. S. *Statistics for Experimenters: An Introduction to Design, Data Analysis, and Model Building*; Wiley: New York, 1978.

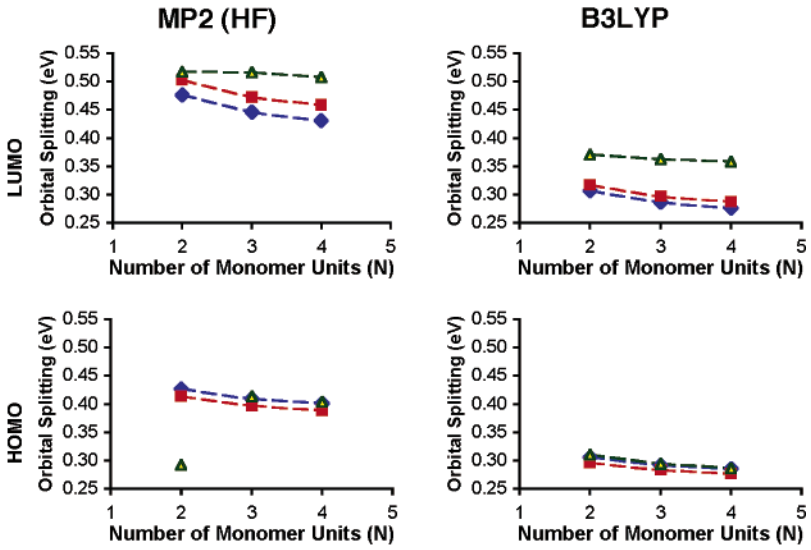

Figure 12. Comparison of HF and B3LYP orbital splittings as a function of oligomer length for LUMO and HOMO orbitals of oligothiophenes (△), oligofurans (■), and oligopyrroles (◆), for cofacial stacking in an eclipsed orientation and with a 4.0 Å intermolecular separation. Note that for both HOMO and LUMO, the splittings decrease, as expected, as a function of oligomer length. The small HOMO splitting for bithiophene using HF appears to be anomalous, and the monotonic trend holds for the B3LYP-computed splittings.

HOMO level splittings similar to those computed by B3LYP or HF here, but smaller LUMO level splittings and an increase in LUMO splitting as a function of oligomer length at this same 4.0 Å intermolecular separation. Since both the B3LYP- and HF-computed splittings computed here agree and do not reveal substantial basis set dependence, we suggest that the previous result is an artifact of the semiempirical INDO method. Even with small basis sets (e.g., 3-21G* and STO-3G) as illustrated in Figure 7, the computed HF orbital splitting energies show the LUMO splitting to be *consistently greater or approximately equal to* the HOMO splitting energy in oligothiophenes. Considering the comparable volumes of the molecular HOMO and LUMO contour maps (Figure 10), it is not clear why in the cofacial eclipsed stacks the overlap of the LUMOs should be substantially different from that of the HOMOs.

Rotation of 180° about the longitudinal molecular axes (*x*-axis) from the eclipsed to inverted conformation decreases the computed LUMO level splittings only slightly, but roughly halves the computed HOMO level splittings. The LUMO splittings are nearly invariant because the inverted configuration places the heteroatoms directly over the β carbon atoms, and both contribute to the LUMO electron density but not to that of the HOMO (Figure 10). These effects are similar in magnitude to those observed previously.[8]

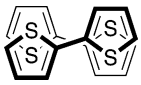

C. Tilt Angle Effects. While the above analysis provides insight into the bandwidth directionality and anisotropy in solid-state oligoheterocycles, all known unsubstituted oligothiophenes and many substituted oligothiophenes do not stack strictly along the Cartesian axes. In particular, in the π-stacking/*z*-axis direction, the molecules often pack in herringbone motifs (e.g., Figure 3) and across the herringbone stacks (along the *d*-axis in Figure 3), one molecule is tilted about the longitudinal molecular axis relative to nearest neighbors, often with tilt angles of ~40−60°.[16−18,32] Such structures[16−18,32] can be modeled by translating one molecule along the *z*-axis, followed by a rotation by an angle θ (about the molecular long axis), moving half of the first molecule closer to the second and half further away. Currently, no single-crystal structures have been reported for oligopyrroles or oligofurans; however, this model represents a reasonable starting place to approximate the packing in these oligoheterocycles, as well. The smaller center-to-center intermolecular spacings (i.e., 4.875 or 5.0 Å) with tilt angles of 40−60° most closely resemble the aforementioned experimental crystal structures. For bithiophene, bifuran, and bipyrrole, the two-dimensional potential energy surfaces were also computed, varying the intermolecular spacings from 4.75 to 6.0 Å and tilt angles (θ) from 0 to 180°.

The computed HOMO and LUMO splittings as a function of tilt angle are shown in Figure 13 for the tetramers of oligomers **1**−**3**. As the two molecules are not symmetrical for arbitrary θ values, the HOMO and LUMO contours of each species may not be exactly identical, resulting in small errors in the computed splitting energies. Nevertheless, recent studies using similar tilted configurations (from crystal structure data) yield excellent agreement between computed and experimental hole mobilities.[14] To systematically compare orbital splittings across all three heterocycles, the cofacial eclipsed (i.e., θ = 0°) orientation is used as the baseline, and Figure 13 illustrates the computed splitting for a given tilt angle as

$$S(\theta) = C(\theta)\, S(0) \qquad (4)$$

where $S(0)$ is the splitting calculated for the given MO at tilt angle θ = 0°, and $C(\theta)$ is the tilting enhancement factor. The splittings approximate Gaussian-like dependence: the overlap increases as one edge of the tilted molecule moves closer to the other, gradually reaching a maximum at 90°, where the two molecules are perpendicular (i.e., as the closest-contact distance decreases, even though the center-to-center distance remains the same). The computed splittings are systematically slightly *smaller* for the inverted (θ = 180°) orientation (likely because this orientation engenders less direct atomic overlap, with one

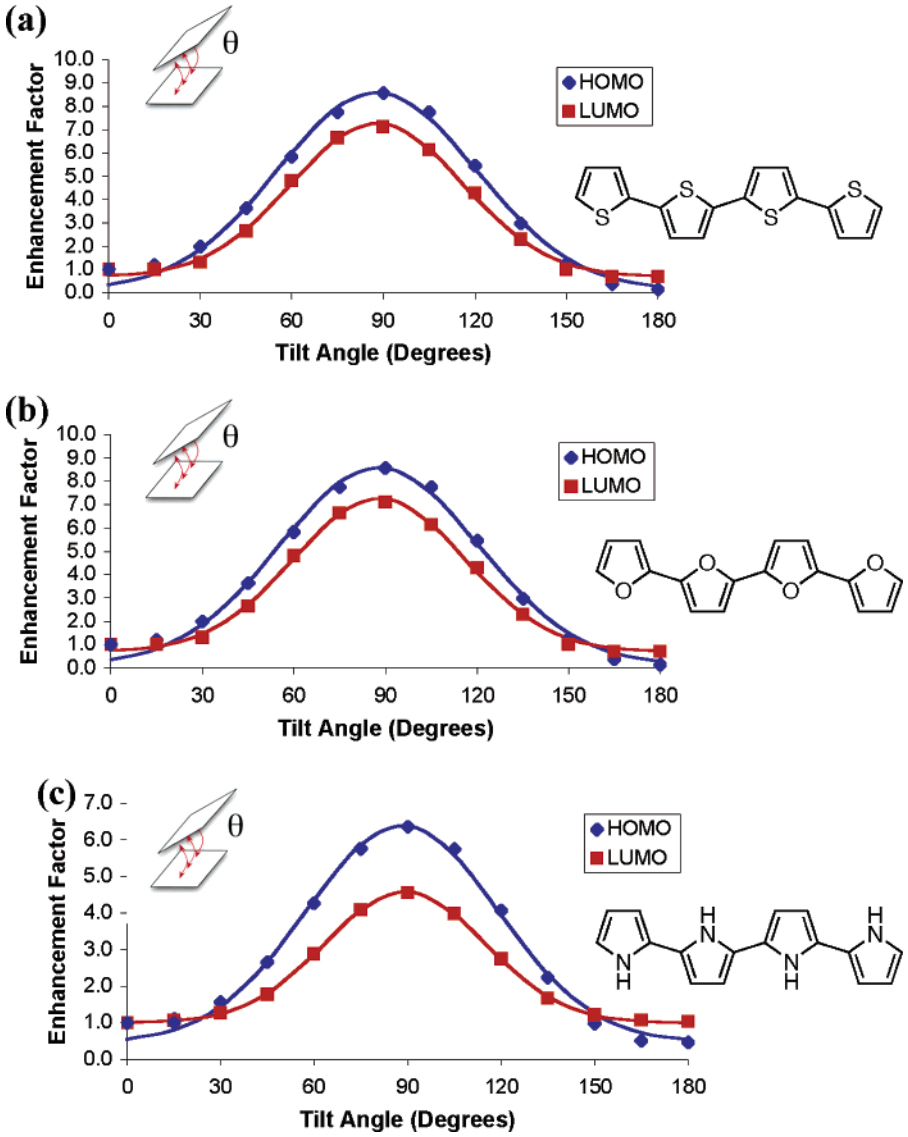

Figure 13. Comparison of HF orbital splittings for tilted π-stacked tetramer dimers as a function of tilt angle (Figure 5) at a fixed 5.0 Å molecular center-to-center distance. Indicated is the "enhancement factor" in splitting—the ratio of the splitting for a given tilt angle to the splitting for the cofacial dimer (tilt angle $\theta = 0°$) for dimers of (a) tetrathiophene, (b) tetrafuran, and (c) tetrapyrrole. Solid lines indicate fits to Gaussian functions, as summarized in Table S3. Note that the actual data are slightly asymmetric, which leads to small deviations in the fits, particularly at small tilt angles for the HOMO levels.

molecule "flipped", directly above the other). Fits to Gaussians are given in Tables S3 and S4, as a function of

$$C(\theta) = y_0 + \frac{A}{w\sqrt{\pi/2}} e^{[-2(\theta - \theta_0)^2/w^2]} \qquad (5)$$

where y_0 is the baseline correction, w is twice the standard deviation or 0.849 times the width at half-maximum, θ_0 is the center of the peak, and A the total area under the curve. Such fits are approximate, as mentioned above; the splittings are smaller at $\theta = 180°$ than at 0°, and so the curve is slightly asymmetric, particularly in the case of the fits to the HOMO enhancements, where the deviation is greatest at small θ.

As seen in Figure 13, the HOMO levels exhibit greater enhancement in splitting with increasing tilt angle than do the LUMO levels. This difference derives from the spatial disposition of the orbitals themselves. In the present frame of reference, increasing the tilt angle changes the relative positions of the short axes of the molecular planes, largely parallel to the HOMOs and largely perpendicular to the LUMOs (cf., Figure 10). This effect is heteroatom-dependent: the oligopyrroles exhibit a slightly smaller increase in both HOMO and LUMO splittings, with the difference between HOMO and LUMO splittings near $\theta = 90°$ increased relative to the oligothiophenes and oligofurans (Figure 13).

The $\theta \neq 0°$ orientations become particularly relevant in view of the computed packing energies. Tilted/herringbone orientations (at a fixed center-to-center distance, e.g., 5.0 Å) are *significantly stabilized* relative to the cofacial eclipsed/inverted orientations—oligofurans and oligopyrroles exhibit binding energies versus $\theta = 0°$ of ~2.0−3.0 kcal/mol per molecular pair for tilted orientations (Figure 14). Across all three oligomer lengths, all oligoheterocycles consistently show two energetic minima in the $\theta \approx 35-60°$ and $\theta \approx 120-135°$ tilt angle ranges. This stabilization relative to the $\theta = 90°$ T-shaped form is greater (~5.0 kcal/mol) for the more electron-rich heterocycles (furan and pyrrole, with smaller ionization potentials and smaller

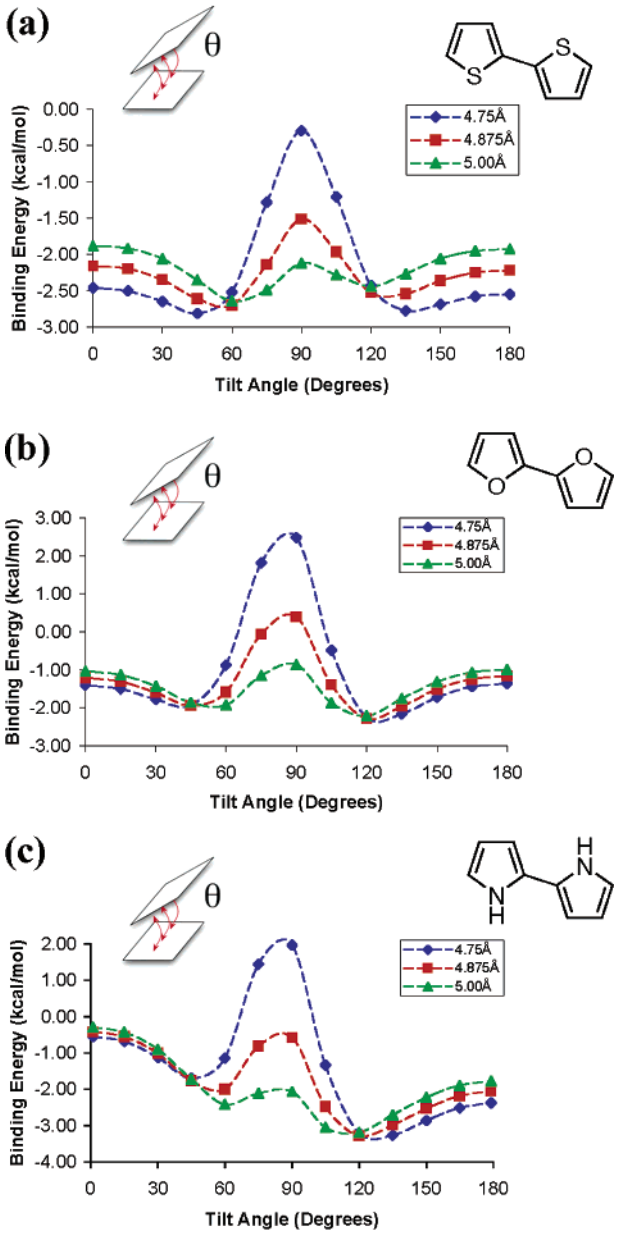

Figure 14. MP2/6-31+G*-computed binding energies with counterpoise corrections of tilted π-stacked oligomers as a function of tilt angle (Figure 5) at a fixed 4.75, 4.875, and 5.0 Å distance between molecular centers as indicated for (a) bithiophene, (b) bifuran, and (c) bipyrrole, respectively. Note that the energetic profiles remain similar in character for all three oligomers; however, the extent of tilted packing stabilization is significantly heteroatom-dependent.

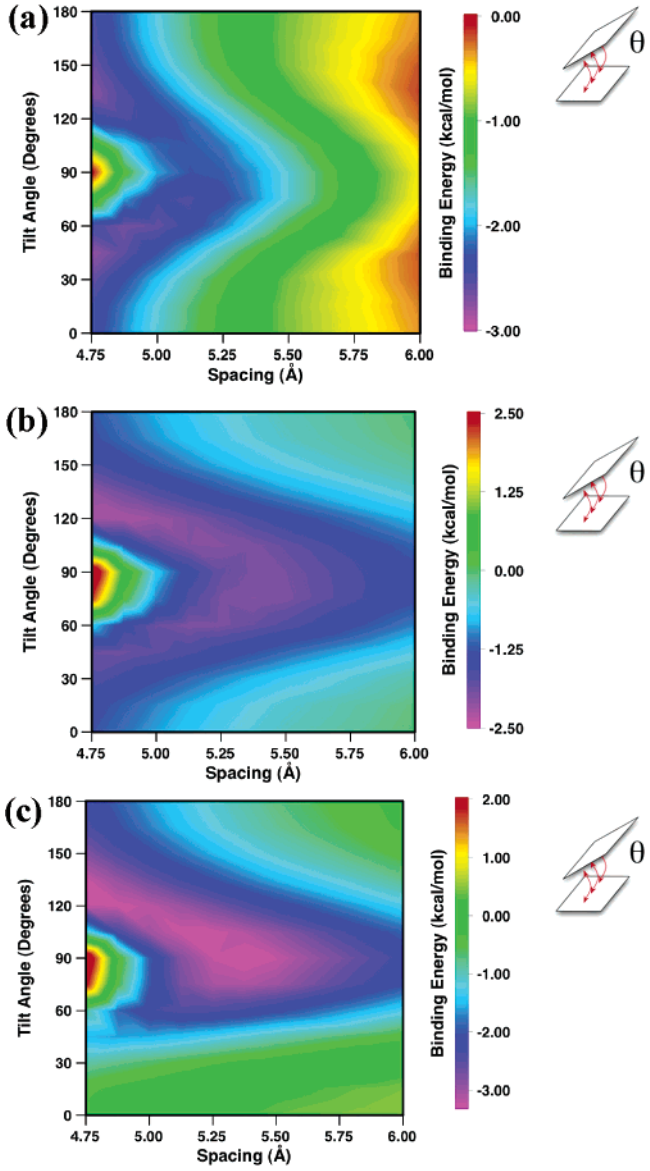

Figure 15. Computed MP2/6-31+G* potential energy surfaces with counterpoise corrections for (a) bithiophene, (b) bifuran, and (c) bipyrrole dimers as a function of intermolecular spacing and tilt angle (Figure 5). Three-dimensional representations may be found in Figure S2.

electron affinities) versus a ~2.5 kcal/mol stabilization for oligothiophenes. While these values are modest, they are consistent across the three oligoheterocycle series as well as across the three oligomer lengths ($n = 2-4$), increasing as a function of oligomer length (e.g., the stabilization for bifuran and bipyrrole is ~50% of that for tetrafuran and tetrapyrrole). The relatively small basis set used for the present MP2 calculations may somewhat underestimate the contribution of dispersion interactions, which are known to be important for $\pi-\pi$ stacking in benzene and in other aromatic systems. Dispersion may contribute additional stabilization for the tilted motifs, as observed for the $\theta = 90°$ benzene dimer.[28,39]

At a center-to-center intermolecular spacing of 5.0 Å and a tilt angle of 60°, the shortest C−C intermolecular contact is smaller for tetrapyrrole and tetrafuran (3.68 and 3.65 Å, respectively) than for tetrathiophene (3.77 Å). This might suggest that at decreased intermolecular separation the oligothiophenes would exhibit greater stabilization energies for the tilted conformations. Indeed, the counterpoise-corrected MP2/6-31+G* potential energy surfaces as functions of intermolecular spacing and tilt angle, illustrated in Figure 15, reveal that for smaller intermolecular separations (i.e., 4.75 Å) the repulsive interactions observed in the perpendicular orientations *increase*—evidently, the oligothiophenes approach too closely, while the tilted form evidences *greater* stabilization. Increasing intermolecular separations for all three oligoheterocycles show that the repulsive interactions observed at ~90° for small separations evolve into stabilization at greater intermolecular separations (e.g., 6.0 Å) probably from attractive van der Waals interactions (Figure 15).

The distance dependence of stabilization is further clarified by examining electron density/electrostatic potential surfaces

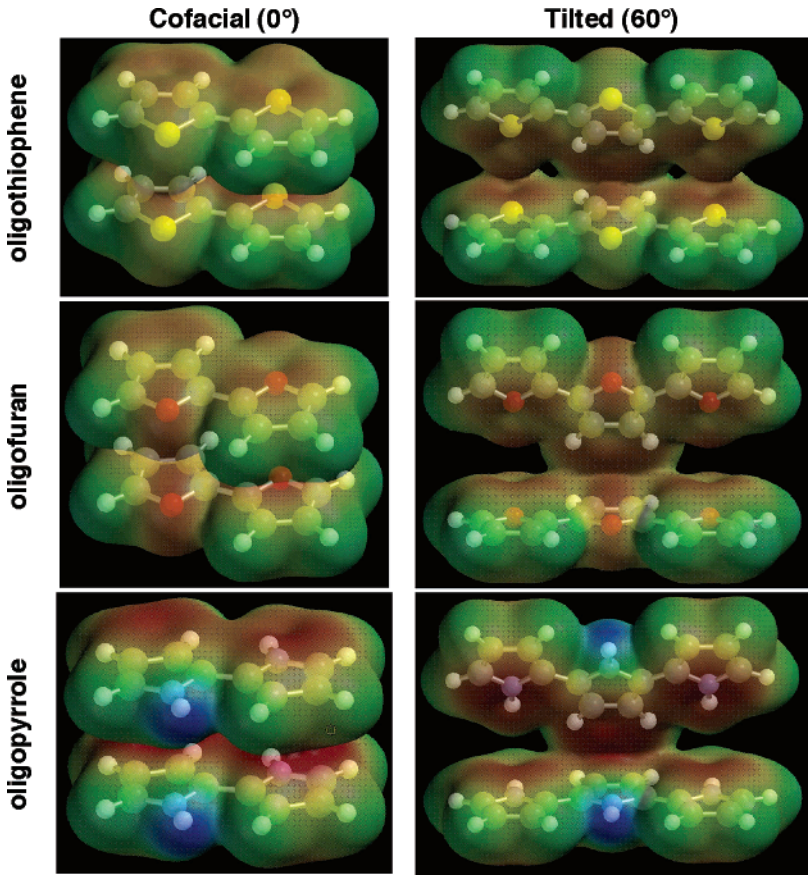

Figure 16. Maps of the DFT electrostatic potential surfaces for cofacial, eclipsed π-stacked dimers (left column), and tilted (60°) π-stacked dimers (right column) of oligothiophenes, oligofurans, and oligopyrroles, all with 5.0 Å molecular center-to-center separations and eclipsed orientations. Red color indicates greater negative charge, while blue color indicates greater positive charge (identical color scale throughout).

for the three oligomers (Figure 16). While the minimum C−C intermolecular distance is larger for oligothiophenes, the greater van der Waals radius of sulfur and the larger molecular width of oligothiophenes along the *y*-axis (Figure 2) yield greater intermolecular π-electron cloud overlap, relative to that of oligofurans and oligopyrroles. The electrostatic potential contours in Figure 16 indicate that the large π-orbital electron density accounts for the repulsive potential energies observed for eclipsed/cofacial arrangements, as discussed above. The electrostatic repulsion is qualitatively lessened in tilted structures, and favorable edge-to-face interactions are incorporated, as well. Electrostatic repulsion in cofacial packings may explain the decrease in orbital overlap with increasing oligomer length as noted above; if the π-orbital volume decreases slightly with increasing oligomer length (to minimize unfavorable electrostatic repulsion which increases with oligomer length), then the bandwidths of cofacial stacks would be expected to similarly decrease with increasing oligomer length. In summary, the present results show that electrostatic effects dominate the packing arrangements and drive molecular pairs away from cofacial π-stacks to tilted forms.

D. Comparisons of Slipped π-Stack Herringbone Models. In addition to the case of tilted π-stacks, which correspond to *d*-axis extension across two herringbone stacks (Figure 3), herringbone π-stacks may also have appreciable hole or electron bandwidths. As described above, the herringbone motif can be considered a slipped-stack, with a translation along the *z*-axis and a "slip" along the *y*-axis (Figure 6), typically on the order of a molecular width (e.g., Figure 3). Figure 17 shows the computed HOMO and LUMO splittings for the tetraheterocycles, as a function of displacement along the *y*- and *z*-axes. Most importantly, the computed LUMO splittings are ~10 times smaller than those in cofacial π-stacks at the same center-to-center displacement (Figure 11), and the HOMO splittings are ~100 times smaller. The smaller HOMO versus LUMO splittings correlate with the same effect observed for coplanar molecules translated along the *y*-axis (Figure 11), likely reflecting the overlap between the heteroatom-centered LUMO portion and the neighboring LUMO residing on C−C backbone fragments. The slipped stacks show reduced repulsive energies relative to cofacial π-stacks, with the stabilization (typically ~0.2 kcal/mol for oligothiophenes and oligofurans, ~2.5 kcal/mol for oligopyrroles) increasing with increasing *z*-axis intermolecular separation and remaining approximately constant with varied *y*-axis intermolecular separation.

E. Consequences for Hole and Electron Transfer Rates. As outlined in the Introduction, overall charge-transfer rates for hopping transport can be described by semiclassical (Marcus) theory based on the internal reorganization energy (λ) and the electronic coupling matrix element, which is half the orbital splitting computed for molecular pairs. This model naturally neglects the possibility of coupling to phonon modes and medium polarization. However, recent applications of the present model to oligothiophenes[13] and pentacene[14] yield reasonable agreement with experimental hole mobility trends. For example, the activation barrier measured experimentally for hole-conduction in single-crystalline sexithiophene is *smaller* than the computed λ,[13,53] which would not be the case if phonon-coupling

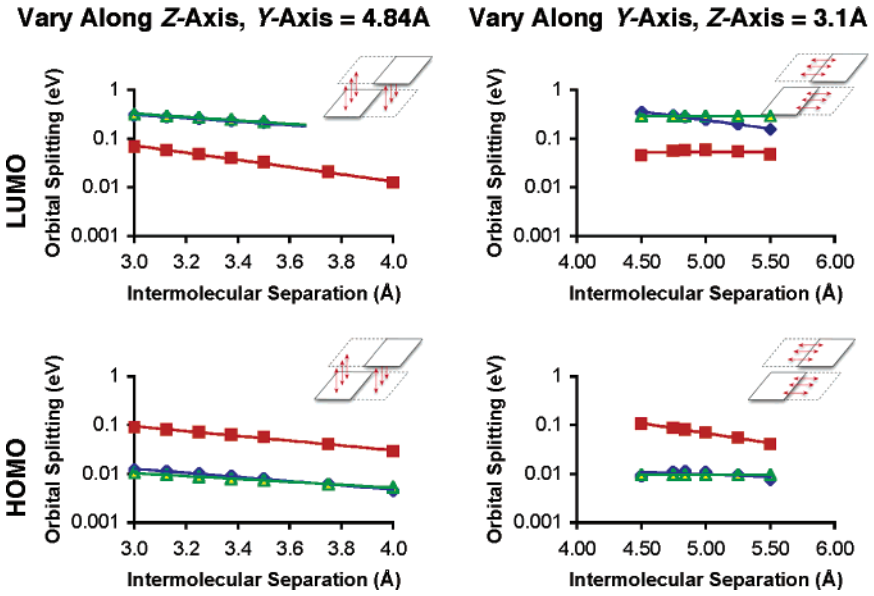

Figure 17. Comparison of the computed HF HOMO and LUMO splittings (on a logarithmic scale) for slipped-stack/herringbone (Figure 6) dimers of tetrathiophene (△), tetrafuran (■), and tetrapyrrole (◆), as a function of center-to-center intermolecular distance along the z/π-stacking direction (left column) at a fixed y-axis displacement and at a fixed z/π-stacking displacement varying the center-to-center intermolecular distance along the y-axis.

Table 3. DFT-Computed Internal Reorganization Energies (in eV) for Oligothiophenes, Oligofurans, and Oligopyrroles ($n = 2-4$) for Both Hole Transfer (λ_+) and Electron Transfer (λ_-)[a]

No. of monomer units	Oligothiophenes		Oligofurans		Oligopyrroles	
	λ_+	λ_-	λ_+	λ_-	λ_+	λ_-
2	0.426	0.395	0.315	0.394	0.353	0.402
3	0.376	0.337	0.292	0.324	0.312	0.319
4	0.342	0.313	0.271	0.286	0.281	0.281

[a] Computed hole transfer λ_+ values are from ref 13.

or polarization effects were significant since these should increase the measured value relative to that computed. Recent computational studies on gas-phase charged oligothiophene dimers suggest only ~0.1−0.2 Å differences in interplanar spacing between neutral and charged dimers,[54] although higher-level calculations suggest that more detailed studies are needed to evaluate the details of such geometric changes.[55]

The reorganization energies for *electron transfer* (i.e., interconversion of neutral and anionic states) have been computed in the present study and are summarized in Table 3, which reveals that the oligothiophene λ parameters for both cations and anions are similar to those reported previously.[56] The λ values computed here for electron transfer in oligothiophenes are slightly smaller than those for hole transfer, in contrast to results for molecules, such as substituted biphenyls.[11] This likely reflects the appreciable reorganization penalty for inter-ring dihedral angle changes in biphenyl radical anions.[11] However, for oligofurans, λ_- is consistently greater than λ_+, while the two are approximately equal for terpyrrole and tetrapyrrole. The oligofurans and oligopyrroles here prefer flat geometries in the neutral, cationic, and anionic states, hence do not incur significant reorganizational barriers from dihedral angle changes even in the gas phase.

Using the computed cation and anion λ values in combination with the HOMO and LUMO orbital splittings in the various packing motifs (cofacial, tilted, slipped π-stacks) presented above, hole and electron transfer rates at 298 K were computed using eq 2, and the results are shown in Figure 18. For cofacial hole transfer, the largest transfer rates are observed for oligofurans, which have the smallest reorganization energies, even though the tight-binding bandwidths are also smallest for oligofurans (Figure 12). While the cofacial hole bandwidths decrease slightly with increasing oligomer length for all three oligomers, the overall hole transfer rates increase significantly for each because the reorganization energies decrease with increasing numbers of monomer units. This implies that variations in intrinsic hole transfer rates with oligomer size or heteroatom are largely governed by variations in the internal reorganization energies because, in the π-stacking direction, the hole bandwidths are quite large and vary by only a few percent with oligomer size and heteroatom (Figures 11 and 12). For example, at an intermolecular separation of 3.5 Å, as used in Figure 18, the bandwidths are ~1.7−1.8 eV (Figure 11). These values are ~44−74% of the intrachain hole bandwidths calculated for infinite polyheterocycles[24] and significantly greater than the bandwidths of ~0.40−0.6 eV measured experimentally in TCNQ[57] or ~0.10−0.50 eV calculated for hole bandwidths in pentacene using various methods.[7,58,59] However, note that the latter molecular cofacial π-stacking is *not* observed in oligothiophene crystal structures.

The picture is slightly different for computed cofacial electron transfer rates since the electron bandwidths computed from LUMO splittings for oligothiophenes are greater than the corresponding hole bandwidths (e.g., 2.1 versus 1.8 eV for terthiophene electron and hole bandwidths, respectively), and

(53) Granstrom, E. L.; Frisbie, C. D. *J. Phys. Chem. B* **1999**, *103*, 8842.
(54) Pickholz, M.; dos Santos, M. C. *THEOCHEM* **2005**, *717*, 99.
(55) Scherlis, D. A.; Marzari, N. *J. Phys. Chem. B* **2004**, *108*, 17791.
(56) Calbert, J.-P.; Brédas, J.-L. Personal communication.
(57) (a) Heeger, A. J. In *Highly Conducting One-Dimensional Solids*; Devreese, J. T., Evrard, R. P., Van Doren, V. E., Eds.; Plenum: New York, 1979; pp 69. (b) Kagoshima, S.; Nagasawa, H.; Sambongi, T. *One-Dimensional Conductors*; Springer-Verlag: Berlin, New York, 1988.
(58) Endres, R. G.; Fong, C. Y.; Yang, L. H.; Witte, G.; Woell, C. *Comput. Mater. Sci.* **2004**, *29*, 362.
(59) (a) Cornil, J.; Calbert, J. P.; Brédas, J. L. *J. Am. Chem. Soc.* **2001**, *123*, 1250. (b) Haddon, R. C.; Chi, X.; Itkis, M. E.; Anthony, J. E.; Eaton, D. L.; Siegrist, T.; Mattheus, C. C.; Palstra, T. T. M. *J. Phys. Chem. B* **2002**, *106*, 8288.

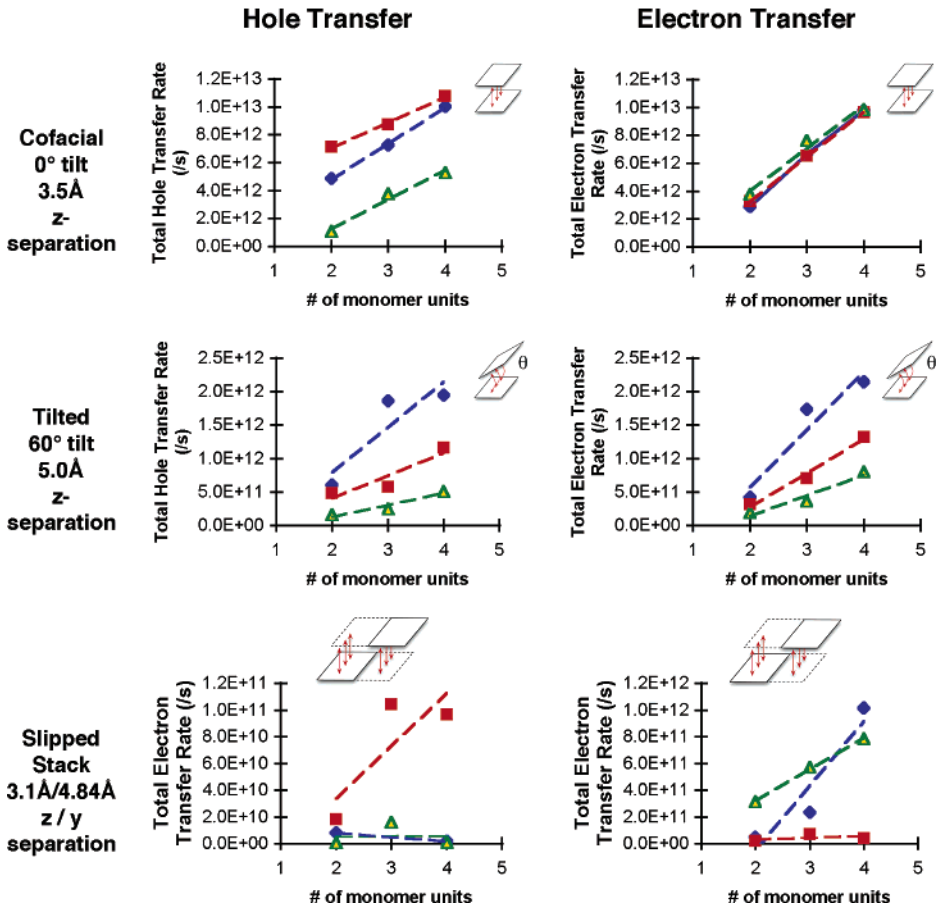

Figure 18. Total computed hole and electron transfer rates for oligothiophenes (△), oligofurans (■), and oligopyrroles (◆) from eq 2, using the internal reorganization energies (λ) calculated for hole and electron transfer from ref 13 and Table 3, respectively, and splittings computed for the z/π-stacking direction in the eclipsed orientation with tilt angles and center-to-center intermolecular separations as indicated (Figure 5) or for the slipped-stack herringbone motif (Figure 6) with the z-axis and y-axis center-to-center intermolecular separations indicated. Geometric parameters approximate those in various oligothiophene crystal structures.

the computed anion internal reorganization energies are smaller. The net result is that computed electron transfer rates are ~2 times greater than the hole transfer rates, while for oligopyrroles and oligofurans, computed electron transfer rates are slightly smaller (~10−20%), primarily because of the greater anion internal reorganization energies relative to those of the cation. In fact, while the oligofurans and oligopyrroles have markedly different electron bandwidths, as illustrated by the LUMO splittings in Figures 11 and 12, the dispersion in computed overall electron transfer rates is only 1−2% (e.g., 9.79×10^{12} and 9.66×10^{12} s^{-1} for tetrafuran and tetrapyrrole, respectively; illustrated in Figure 18) because the computed anion reorganization energies effectively compensate.

For the tilted π-stacking arrangements, as noted above, oligopyrrole structures have significantly greater bandwidths than do either the oligothiophenes or oligofurans and hence have greater computed hole and electron transfer rates, although again, the increase in computed charge-transfer rate with increased oligomer length is driven by a 2−3-fold increase in the exp($-\lambda/4k_BT$) reorganization energy term. Similarly, the oligofuran cation reorganization energies are systematically smaller than those of the oligothiophenes, and the computed hole transfer rates are correspondingly greater for the oligofurans, while the opposite is observed for electron transfer rates. For all tilted configurations, the computed bandwidths are greater than those for a simple cofacial arrangement at the same center-to-center intermolecular spacing (Figure 13; even though a portion of the tilted molecule is further away) but smaller than those for a cofacial π-stack in which the intermolecular distance is fixed at the closest (but unstable—vide supra) C−C contact for the tilted form.

For slipped stacks arrayed along herringbone directions, computed hole transfer rates are ~10 times smaller than that for tilted π-stacks because of the significantly smaller bandwidths. The small variations are a significant percentage of the total bandwidth and thus yield noticeable variations in computed hole transfer rates (Figure 18). On the other hand, the greater electron bandwidths in the slipped π-stacks yield computed electron transfer rates comparable to those of tilted π-stacks, with the exception of the oligofurans. The electron bandwidths remain relatively constant as a function of oligomer length, yet the electron transfer rates increase since the λ barrier decreases in longer oligomers.

The importance of λ in these systems is significant, largely because in the π-stacking direction, either cofacial or tilted intermolecular arrangements have significant computed bandwidths for both holes and electrons. For other directions, such as along the x or y Cartesian axes, the computed bandwidths are ~2−3 orders of magnitude smaller, which results in 4−6 orders of magnitude decrease in computed charge-transfer rates. The overall picture of charge transfer in these materials, from the computed dimer charge-transfer rates, is an anisotropic one,

with almost all charge transfer in the π-stack directions and λ acting as the rate-determining barrier in these directions. Indeed, in thin single-crystal sexithiophene measurements,[53] thermally activated hole transport is observed at temperatures above 100 K with an activation barrier of 0.025 eV, in reasonable agreement with the computed gas-phase barrier ($\lambda/4$).[13] This implies that the lattice environmental reorganization (akin to outer-sphere reorganization energy in solution-phase charge-transfer processes) is very small, as assumed above; otherwise, the experimental activation barrier would be larger than the computed one.

For both the cofacial and herringbone π-stack orientations, the differences between computed hole and electron transfer rates are largely driven by changes in internal reorganization energies—computed hole and electron bandwidths are within 20% of each other for all three heterocycles and oligomer lengths considered. This suggests that the relative paucity of *n*-type conductive/semiconductive organic materials with high mobilities[16,60] compared to *p*-type ones is *not* accounted for by differences in relative hole and electron bandwidths in these materials, particularly for unsubstituted oligoheterocycles. Other recent first-principles band-structure calculations on pentacene and other conjugated materials confirm that computed electron bandwidths can be greater than hole bandwidths and computed electron effective masses can be smaller than hole effective masses.[50,58]

IV. Conclusions

The necessary requirement for *electrically conductive* organic materials is the ability to efficiently transfer charge, either via holes or via electrons, between neighboring units. Therefore, we have considered hopping-type transport between two neighboring conjugated heterocyclic oligomers as an electron-transfer reaction and focused on the influence of structural variables, such as intermolecular separation, intermolecular orientation, heteroatom identity, and oligomer length on the computed electronic coupling for hole and electron transfer between neighboring units.

The present first-principles analysis provides considerable insight into the relative energetics of various oligoheterocycle packing motifs and the resulting bandwidths for charge transfer. The relative computed energies of intermolecular organization in these oligoheterocycles agree well with the motifs observed experimentally in oligothiophene single crystals and suggest that the tilt angles in herringbone stacks reflect minimization of electrostatic repulsions and incorporation of favorable edge electrostatic attraction, as in the benzene dimer.[28,29] The stabilization energies of the tilted π-stack structures increase as a function of oligomer length and are larger for the more electron-rich (i.e., smaller ionization potential and smaller electron affinity) oligofurans and oligopyrroles. The computed bandwidths, represented by twice the HOMO and LUMO splittings in the oligomer pairs, suggest that the bare electron bandwidths in these materials are greater than those computed by previous semiempirical calculations. Computed bandwidths exhibit non-negligible dependence on heteroatom identity and oligomer length.

The variation in orbital splittings with increased molecular tilt angle is in accord with increased overlap resulting from decreased intermolecular contact distances (i.e., while the center-to-center distance remains the same, the closest-contact distance changes). This increases both hole and electron bandwidths, although the effect is greater for the former than for the latter due to the LUMO special distributions in these oligoheterocycles (Figure 10). The increased bandwidths with increased tilt angles means that the tilted forms exhibit hole/electron bandwidths $\sim$33−50% of those for eclipsed cofacial stacking at the smallest interplanar separation, but are energetically more stable. The slipped π-stack motifs have significantly smaller hole bandwidths and somewhat smaller electron bandwidths, suggesting that the anisotropy of charge transport in *p*- and *n*-type slipped-stack materials is likely to be different.

The hole and electron transfer rates computed in this study suggest that the intrinsic hole and electron mobilities in these unsubstituted oligoheterocycles can be comparable, so that observed differences between charge-transfer rates for particular systems are largely governed by differences in internal reorganization energies. Since the cation and anion reorganization energies for these species are also comparable, many of the observed differences in *n*-type and *p*-type performance in conductive/semiconductive organic materials must be due to other contributing effects, such as charge injection, traps, or grain boundary scattering. Future work will focus on chemical modification of internal reorganization energies, for example, with heterocycle substituents, since these are of clear importance for understanding trends in intrinsic charge mobility in organic conductors.

This work addresses several key issues in current organic electronic materials research, including the following: (1) a detailed comparison of the electron and hole bandwidths demonstrates that the paucity of *n*-type organic conductive materials is *not due to intrinsically small electron bandwidths* (and thus to inadequate *n*-type charge mobility) in these materials; (2) computed overall intrinsic charge-transfer rates for electron and hole transport are *essentially equal* except in the slipped-stack direction, where hole transport decreases significantly; and (3) an MP2-based framework is presented to facilitate analysis of oligoheterocycle families, in which there is a paucity of solid-state structural data.

Acknowledgment. We thank the NSF/MRSEC program through the Northwestern MRSEC (NSF DMR-0076097), the ONR (N00014-02-1-0909), and the NASA Institute for Nanoelectronics and Computing (Award NCC 2-3163) for support. This work was also supported in part by a computer resource grant from the University of Minnesota Supercomputing Institute in conjunction with the 2002 IBM Computational Chemistry Award of the Subdivision of Theoretical Chemistry of the American Chemical Society.

Supporting Information Available: Complete ref 26, tables of MP2 (HF) and B3LYP-computed orbital splittings for the three Cartesian axes (S1 and S2, respectively) and the tilted π-stacked oligomers (S3 and S4). Figures comparing HF and B3LYP orbital splittings (S1) and three-dimensional representations of the tilted potential energy surfaces (S2). This material is available free of charge via the Internet at http://pubs.acs.org.

JA0533996

(60) (a) Chesterfield, R. J.; Newman, C. R.; Pappenfus, T. M.; Ewbank, P. C.; Haukaas, M. H.; Mann, K. R.; Miller, L. L.; Frisbie, C. D. *Adv. Mater.* **2003**, *15*, 1278. (b) Pappenfus, T. M.; Chesterfield, R. J.; Frisbie, C. D.; Mann, K. R.; Casado, J.; Raff, J. D.; Miller, L. L. *J. Am. Chem. Soc.* **2002**, *124*, 4184. (c) Facchetti, A.; Mushrush, M.; Yoon, M.-H.; Hutchison, G. R.; Ratner, M. A.; Marks, T. J. *J. Am. Chem. Soc.* **2004**, *126*, 13859.